CHALMERS

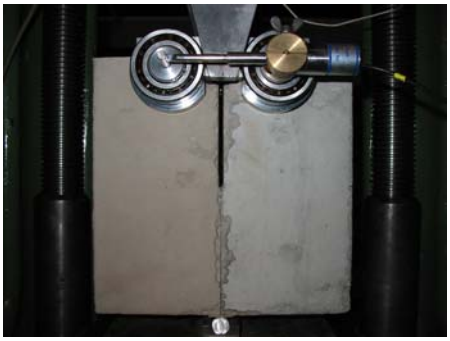

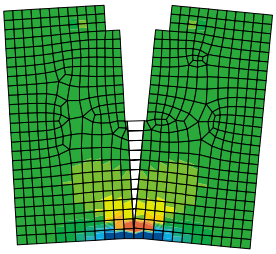

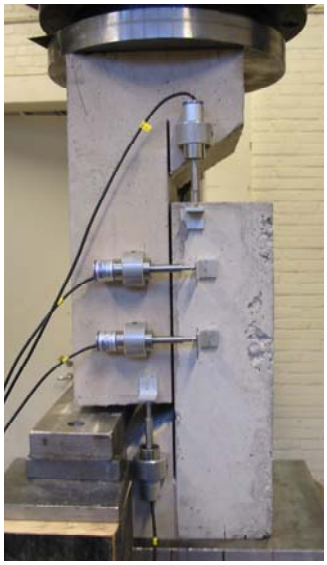

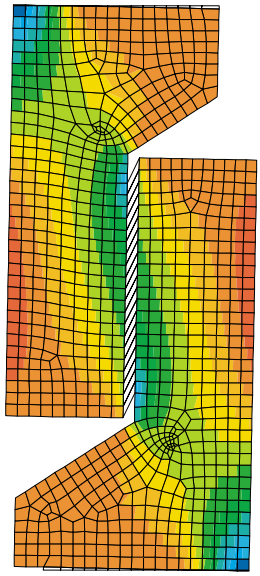

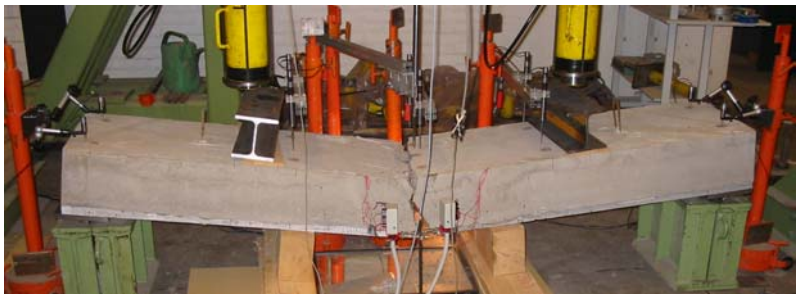

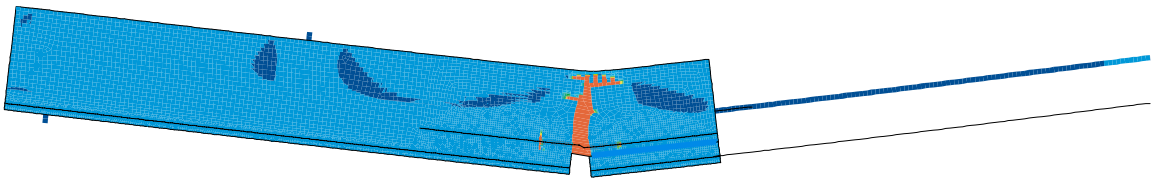

Joints in lattice girder structures

KARIN LUNDGREN, JOHAN HELGESSON,
RASMUS SYLVÉN

Department of Civil and Environmental Engineering
Division of Structural Engineering
Concrete Structures
CHALMERS UNIVERSITY OF TECHNOLOGY
Göteborg, Sweden 2005

Report 2005:9

REPORT 2005:9

Joints in lattice girder structures

KARIN LUNDGREN, JOHAN HELGESSON,

RASMUS SYLVÉN

Department of Civil and Environmental Engineering
Division of Structural Engineering
Concrete Structures
CHALMERS UNIVERSITY OF TECHNOLOGY
Göteborg, Sweden 2005

Joints in lattice girder structures

KARIN LUNDGREN, JOHAN HELGESSON,
RASMUS SYLVÉN

ISSN 1652-9162
Report 2005:9
Department of Civil and Environmental Engineering
Division of Structural Engineering
Concrete Structures
Chalmers University of Technology
SE-412 96 Göteborg
Sweden
Telephone: + 46 (0)31-772 1000

Cover:
Wedge split tests, shear tests and full-scale tests and analyses of them

Department of Civil and Environmental Engineering
Göteborg, Sweden 2005

Joints in lattice girder structures

KARIN LUNDGREN, JOHAN HELGESSON,
RASMUS SYLVÉN
Department of Civil and Environmental Engineering
Division of Structural Engineering
Concrete Structures
Chalmers University of Technology

ABSTRACT

To enable load-carrying in two directions in lattice girder systems, transverse reinforcement in the precast concrete panels needs to be complemented with lapped reinforcement across the joints at the construction site. To ease production, it would be beneficial not to have any reinforcement across the cast joint between the precast concrete and the *in situ* cast concrete within the splice region. However, this raises questions whether the cast joint will manage to transfer the needed forces. This was studied in the present project. Two different surface treatments of the precast elements were studied: one was brushed and the other had single grooves. In the studied detailing of the joint, a reinforcement mesh was placed in the *in situ* concrete across the joint, directly on the surface of the precast elements between the lattice girder trusses.

Two types of detail tests of the cast joint were carried out: one type where the cast joint was loaded in shear and one in tension. Furthermore, the detailing of the joint between two precast concrete panels was tested in bending in full-scale tests. The detail tests were used to calibrate a model of the cast joint, which was then used in non-linear finite element analyses of the full-scale tests. The test specimens with surfaces with single grooves showed a large scatter in the detail tests loaded in shear; in all other tests the scatter was relatively low. Furthermore, the capacity of the cast joint was markedly higher for the brushed surface than for the surface with single grooves.

In the full-scale tests, the joints were strong enough to carry the applied load. In all full-scale tests the failure mode was rupture of the reinforcement, and only one crack occurred: in the *in situ* cast concrete above the joint between the precast elements. However, the finite element analyses of the full-scale tests revealed that the detailing was sensitive for secondary cracking; when restraints from the cross-bars of the reinforcement mesh initiated bending cracks, the failure mode changed to fracture of the cast joint in the analyses. This happened in the analyses where the precast surface was modelled with single grooves. In the analysis where the surface was modelled as brushed, no secondary cracking occurred even when the restraints from the crossbars were included in the analyses. It is worth to note that in the full-scale tests, the cross-bars were placed directly on the surface of the precast concrete; accordingly they were most likely not so well encased and did not cause any larger restraints. Measurements of the strains in the reinforcement support this.

Analyses of whole slabs were carried out to investigate the demands of the deformation capacity of the lattice girder joint. They showed that the load-carrying capacity of a slab depends on the rotation capacity of the lattice girder joints. Therefore, it is recommended that the rotation capacity is not limited by the horizontal cast joint.

From the results in this study, it was concluded that the studied detailing of load-carrying joints between lattice girder slabs without any reinforcement across the cast joint is very sensitive to the roughness of the surface of the prefabricated elements. There is a risk of brittle failures; thus it raises questions whether reinforcement across the cast joint is needed to guarantee the structural integrity of a structure. It is further concluded that not all surfaces of the prefabricated elements used in Sweden today can be used. Considering this, it might however still be possible to use the studied detailing for load-carrying purposes. Very important demands are then that both the production of the surface of the prefabricated elements and the conditions at the work site must be controlled and checked on regular basis.

Long-term effects such as shrinkage and creep were not included in the present study. This needs to be investigated. Furthermore, it is recommended that detailings with reinforcement across the cast joint are investigated, as the structure would become a lot more robust if that is included.

Key words: Cast joint, lattice girder, prefabricated concrete element, load-carrying in two directions, joint, wedge split test (WST), shear test, finite element analyses, splice.

Fogar i plattbärlag

KARIN LUNDGREN, JOHAN HELGESSON, RASMUS SYLVÉN
Institutionen för bygg- och miljöteknik
Avdelningen för konstruktionsteknik
Betongbyggnad
Chalmers tekniska högskola

SAMMANFATTNING

Plattbärlag är ett kompositbjälklag av prefabricerade betongelement och platsgjuten betong. För att möjliggöra bärning i två riktningar i plattbärlag, måste armering i den prefabricerade delen kompletteras med skarvarmering över fogarna på byggplatsen. För att underlätta produktionen vore det fördelaktigt att inte ha någon armering som korsar den horisontella gjutfogen mellan den prefabricerade och den platsgjutna betongen inom skarvområdet. Detta ställer dock krav på att gjutfogen klarar av att överföra de krafter som behövs. Denna frågeställning studerades i detta projekt. Två olika ytbehandlingar på de prefabricerade elementen studerades: en var borstad, och en hade enstaka räfflor. I den studerade utformningen av fogen var ett armeringsnät placerat i den platsgjutna betongen, direkt på den prefabricerade betongens yta mellan plattbärlagets armeringsstegar.

Två sorters detaljförsök på gjutfogen utfördes: en där gjutfogen belastades i skjuvning, och en där den belastades i drag. Dessutom provades fogar mellan två plattbärlag i fullskaleförsök, belastade i böjning. Detaljförsöken användes för att kalibrera en modell av gjutfogen. Denna modell användes sedan i icke-linjära finita elementanalyser av fullskaleförsöken. Provkropparna med ytor med enstaka räfflor hade en stor spridning i resultaten i detaljförsöken belastade i skjuvning. I alla de övriga försöken var spridningen relativt liten. Dessutom var kapaciteten för gjutfogen betydligt högre för den borstade ytan än för ytan med enstaka räfflor.

I fullskaleförsöken visade sig fogarna vara starka nog för att bära den pålagda lasten. Brottmoden i alla fullskaleförsöken var avslitning av armeringen, och bara en spricka uppstod: i den platsgjutna betongen över fogen mellan plattbärlagselementen. Finita element analyser av fullskaleförsöken visade dock att detaljen är känslig för sekundära sprickor – när tvång från tvärstängerna i armeringsnäten initierade böjsprickor förändrades brottmoden till brott i gjutfogen. Detta inträffade i analyserna där ytan på de prefabricerade elementen modellerades med enstaka räfflor. I analyser där ytan på de prefabricerade elementen modellerades som borstad inträffade inga sekundära sprickor ens när tvång från tvärstängerna var inkluderade i analysen. Det är värt att notera, att i fullskaleförsöken var armeringsnäten placerade direkt på ytan på den prefabricerade betongen – på grund av detta var de förmodligen inte så väl kringgjutna och orsakade inte något större tvång. Mätningar av töjningar i armeringen stödjer detta.

Analyser av hela bjälklag utfördes för att undersöka vilka deformationskrav som bör ställas på en fog mellan plattbärlagselementen. Analyserna visade att bjälklagets lastkapacitet beror på fogarnas rotationskapacitet. Därför bör inte fogens rotationskapacitet begränsas av den horisontella gjutfogen.

Resultaten i denna studie visade att det studerade detaljutförandet på lastbärande fogar mellan plattbärlagselement utan armering i den horisontella gjutfogen är väldigt känsligt för skrovligheten hos ytan på de prefabricerade elementen. Det finns risk för spröda brott, och detta gör att man kan ifrågasätta om det inte behövs armering tvärs gjutfogen för att garantera säkerheten. Vidare visar resultaten att inte alla ytor på prefabelement som används i Sverige idag bör användas. Med detta i åtanke, kan det dock fortfarande finnas en möjlighet att använda den studerade detaljen som lastbärande. Om så skall göras, är det väldigt viktigt med krav på att både produktionen av ytan av det prefabricerade elementet, och förhållandena på byggplatsen, styrs och kontrolleras regelbundet.

Långtidseffekter såsom krypning och krympning var inte inkluderade i denna studie. De bör därför undersökas. Ytterligare en rekommendation för framtida forskning är att undersöka utföranden som inkluderar armering som korsar gjutfogen. Därigenom skulle konstruktionen bli betydligt robustare, och kontrollbehovet både på fabrik och på byggplats skulle minska. I en sådan undersökning är det viktigt att ta fram armeringsutformningar som ger ett rationellt arbetsutförande på byggplatsen.

Nyckelord: Gjutfog, plattbärlag, förtillverkade betongelement, lastbärning i två riktningar, fog, spricköppningsförsök, skjuvförsök, finita element analyser, skarv.

Contents

Preface

In this study, the structural behaviour of joints in lattice girder structures were investigated. Experimental work, including full-scale tests of lattice girder structures and detail tests of grouted joints, was combined with finite element analyses. The work was carried out from May 2004 to March 2005. The project was initiated and partly financed by "Svenska Fabriksbetongföreningens plattbärlagsgrupp", and also financed by the Development Fund of the Swedish Construction Industry (SBUF) and Fundia Hjulsbro AB. The work has been followed by a reference group consisting of representatives from "Svenska Fabriksbetongföreningens plattbärlagsgrupp". Furthermore, FoU-Väst (a group of representatives from the building industry in western Sweden dealing with research and development) has also been involved as a reference group.

Parts of the work were carried out within a master thesis project by Johan Helgesson and Rasmus Sylvén, see Helgesson and Sylvén (2005). The thesis work was supervised and the other parts of the work were carried out by Karin Lundgren. In the master thesis project, the calibration of the model of the cast joint was by mistake done with wrong loaded area. Therefore this was changed here, which led to a completely new calibration of the model of the cast joint, and consequently the results in the analyses of the full-scale tests were changed compared to what was reported in the master thesis report.

The prefabricated parts of the test specimens were manufactured and supplied by Abetong and Hedareds Sand & Betong. All tests were carried out in the laboratory of the Department of Structural Engineering and Mechanics at Chalmers University of Technology. We are most grateful to Lars Wahlström, who made most of the practical work with the experiments. We would also like to thank Ingemar Löfgren and Mario Plos for interesting discussions about the studied problem, and for reading and commenting this report.

Göteborg May 2005

Karin Lundgren, Johan Helgesson and Rasmus Sylvén

Notations

Roman letters

c	Concrete cover
D_{11}, D_{22}	Elastic stiffnesses
d	Distance between reinforcement mesh and top of the in situ concrete
F_v	Vertical load
F_{sp}	Horizontal splitting force
f_{cc}	Compressive strength
f_{ct}	Tensile capacity
G_F	Fracture energy
P	Point load
u_n	Normal deformation
u_t	Slip deformation
w	Crack opening

Greek letters

α	Wedge angle
δ	Mid-deflection
η	Dilation parameter
κ	Hardening parameter
μ	Friction coefficient
σ_n	Normal stress
τ	Bond stress

1 Introduction

The lattice girder system is a semi-precast element floor, where precast concrete panels are combined with in-situ concrete topping, see Figure 1. Lattice girder systems can either be load-carrying in only one direction, or in two directions. To enable load-carrying in two directions, there are two possibilities:

1. Transverse reinforcement is placed on the precast concrete panels on the construction site. The transverse reinforcement bars must then be pulled through the lattice girders, which is time-consuming.

2. The second alternative is to put transverse reinforcement in the precast concrete panels. This must be complemented with lapped reinforcement across the joints at the construction site.

In the work presented here, the second alternative is investigated. The aim with this study is to investigate the behaviour and capacity of a joint where the spliced reinforcement consists of mesh between the lattice girder trusses, without any reinforcement crossing the cast joint as shown in Figure 2. This was studied through a combination of experiments and non-linear finite element analyses. Detail tests of the cast joint between the precast and the *in situ* concrete were carried out; by analysing these tests a model of cast joint could be calibrated. This model of the cast joint was then used in analyses of a lattice girder structure, which was also tested in full-scale experiments. Two types of surfaces of the precast elements were tested and analysed: a brushed surface and a surface with single grooves.

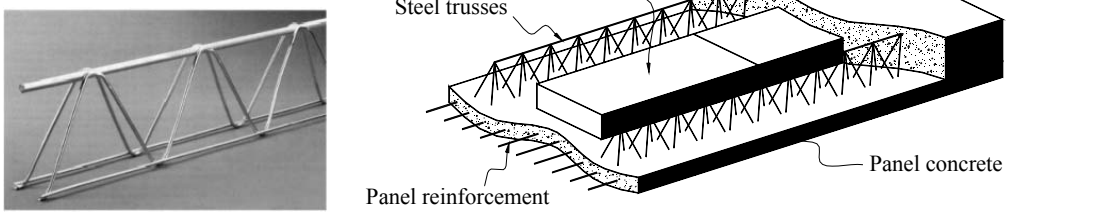

Figure 1 A lattice girder truss and a lattice girder element.

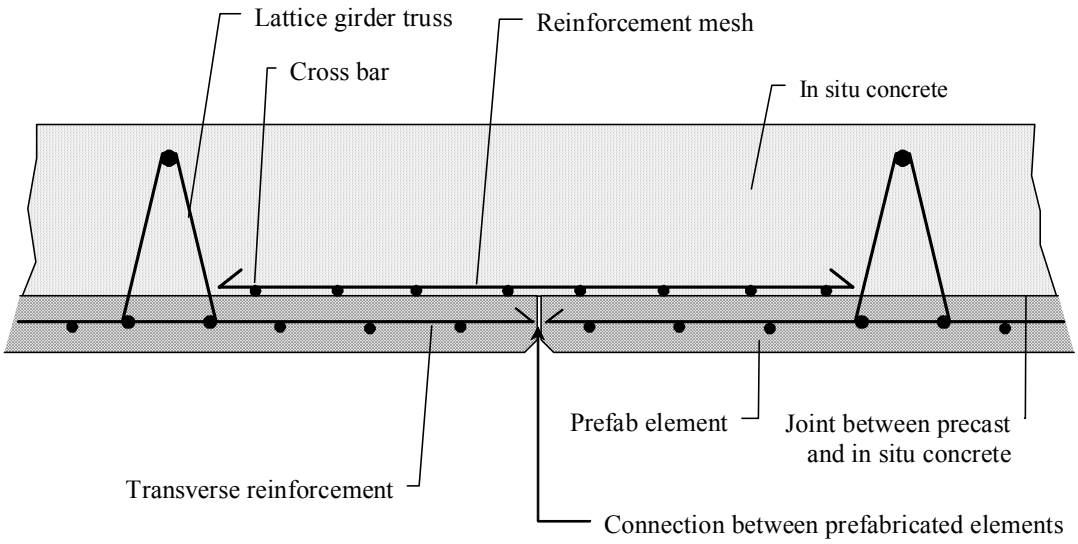

Figure 2 Example of a splice in the joint between two lattice girder elements.

2 Experiments

In this chapter, the test specimens, experiments and test results are presented. The tests were performed at the laboratory at Chalmers University of Technology, Structural Engineering and Mechanics. Three types of tests were carried out: shear, wedge split and full-scale tests of lattice girder structures. The two first tests were used to calibrate the joint behaviour in the finite element analyses. Further information about the tests and results can be seen in respective section.

2.1 Manufacturing of test specimens

Two manufacturers made the prefabricated concrete elements: Abetong and Hedareds Sand & Betong. These two manufacturers were chosen to get a good overall figure of the surface among the lattice girders used in Sweden. Abetong should represent a smooth surface and Hedared a rougher surface on the lattice girder. Abetong made grooves with about 100 mm distance and a depth of about 10 mm. Hedareds Sand & Betong used a steel brush to make the surface rough. The depth of the roughness was approximately 7 mm over the whole surface. For photographs of surfaces and number of grooves of each element see Appendix A.

The prefabricated parts of all the test specimens were cast at the same time, at 17th September 2004 at both manufacturers. However, by mistake the shear test specimens from Hedareds Sand & Betong were brushed in the wrong direction. Therefore, new shear test specimens were made by that manufacturer about a week later. The prefabricated components were delivered to the laboratory at Chalmers when they were 4-7 days old. There, preparations for the *in situ* concrete casting were done.

The reinforcement units between the lattice girder trusses were provided with strain gauges. After completing of formworks, the *in situ* concrete was cast at the 1st October 2004. Thus, the prefabricated concrete had hardened for fourteen days, when the *in situ* concrete was cast, except for the shear test specimens from Hedareds Sand & Betong which had hardened for a week. The *in situ* cast concrete was for all specimens cast on top of the prefabricated concrete.

2.2 Material properties

The composition of the concrete is shown in Table 1.

At each grouting (except for the extra grouting of the shear test specimens at Hedareds Sand & Betong), nine cylinders ($150 \times 300\,\text{mm}^2$) were cast from the actual batch of concrete. The cylinders were wet stored until they were tested. Three from each batch was tested when the test series started, and three were tested when the experimental work was finished, see Table 2. The remaining three cylinders from each batch were not tested; they were cast to have a possibility to test them if the experimental work for some reason would take much longer time than expected.

Table 1 Composition of concrete.

	Abetong	Hedared	*In situ*
Water [kg/m^3]	160	179	207
Cement [kg/m^3]	340	449	405
0-8 mm [kg/m^3]	1200	925	902
8-16 mm [kg/m^3]	624	695 [1)]	829
Admixture [kg/m^3]	3.7 [2)]	1.6 [3)]	-

[1)] 8-11 mm
[2)] Cemflux Prefab
[3)] Adva Flow 341

*Table 2 The compressive strength of the concrete tested on wet stored cylinders, 150*300 mm^2. Each value is an average of three tests.*

Concrete	Cast	Tested	Age [days]	f_{cc} [MPa]
Abetong	17-Sept	11-Nov	55	48.7
	17-Sept	2-Dec	76	51.4
Hedared	17-Sept	1-Nov	45	56.7
	17-Sept	2-Dec	76	60.1
In situ	1-Oct	1-Nov	31	36.0
	1-Oct	2-Dec	63	40.8

The properties of the reinforcement mesh was tested in three tensile tests on specimens with a loaded length of 400 mm. The resulting force versus strain is shown in Figure 3. For strains below 6-7 ‰, measurements from strain gauges were used; while larger strains were calculated as the total deformation divided by the length.

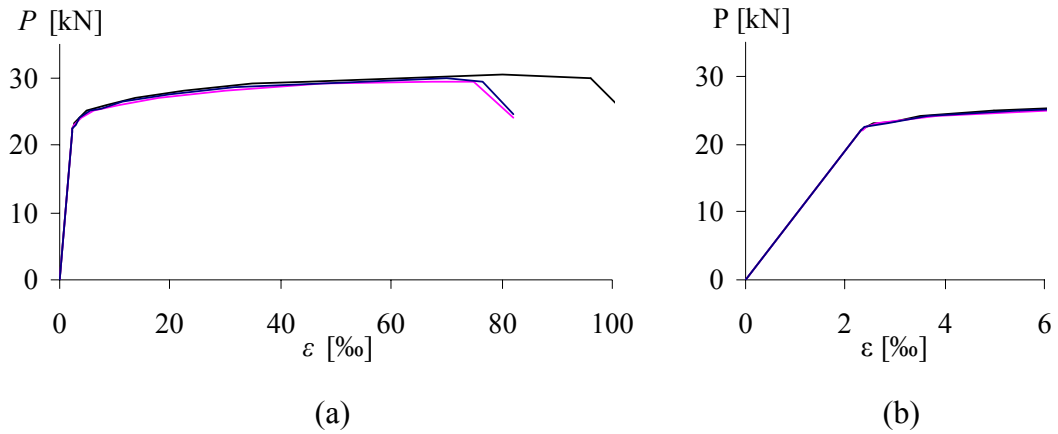

Figure 3 *Tensile force versus strain in tests of reinforcement mesh. (a) Whole curve; (b) enlargement of first part.*

2.3 Shear tests

2.3.1 Test specimens

The joint behaviour at loading was of great importance when modelling the joint. In the first part of this project Lundgren (2003) used a friction model calibrated by tests by Nissen *et al.* (1986). There were still some uncertainties with this model and calibration, thus two new types of tests were performed.

The geometry of the shear test specimens was similar from both suppliers, while treatment of the surface differed between the two manufacturers. The shear test specimens were provided with stirrups to avoid concrete from splitting at loading. For details and drawings, see Figure 4.

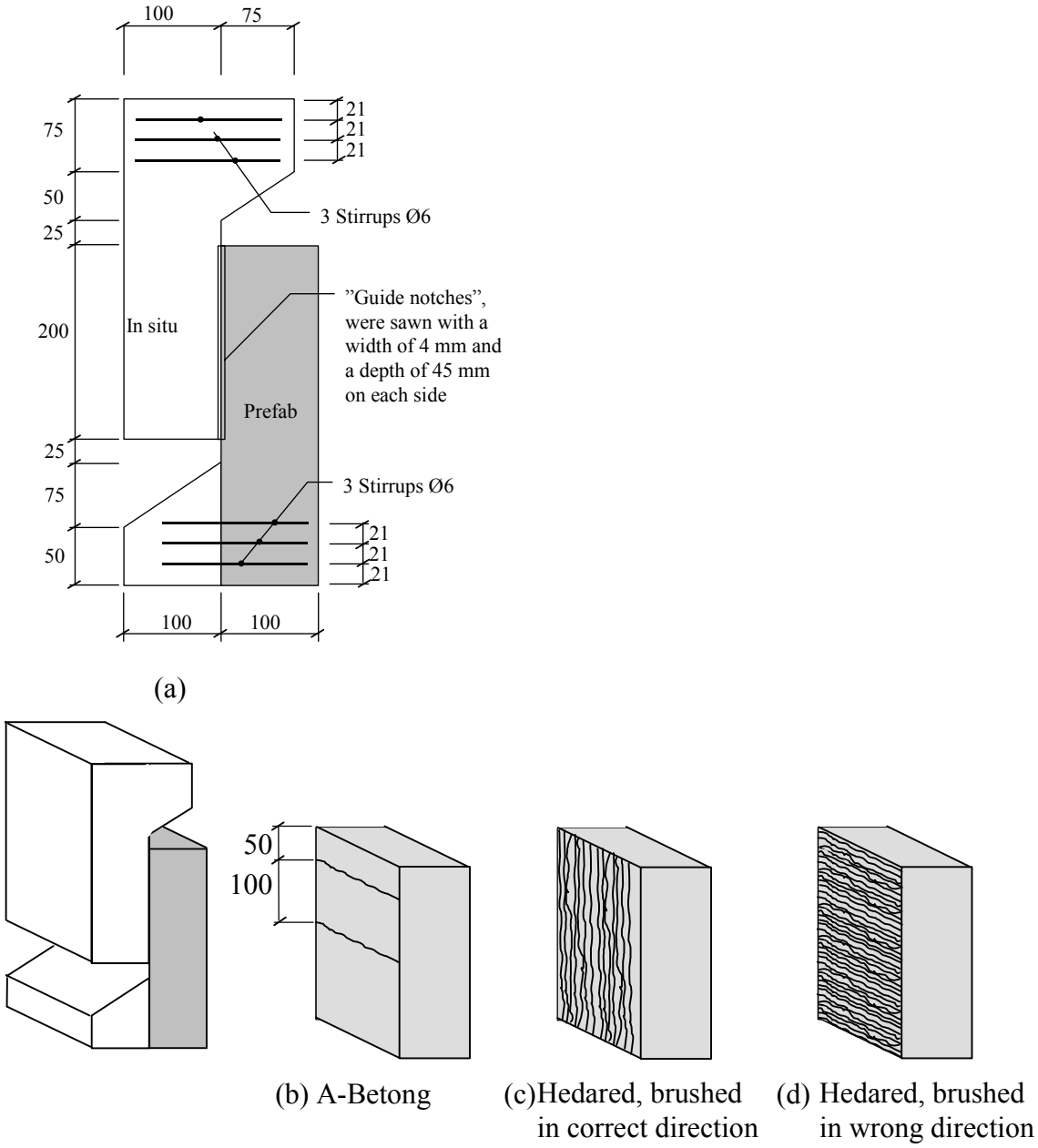

Figure 4 *Geometry of shear test specimens, (a) whole specimens; (b-d) treatment of surface of prefabricated concrete.*

Hedareds Sand & Betong treated the surface to a homogenously brushed roughness. By mistake, the surfaces of the shear test specimens from Hedared were brushed in wrong direction. Therefore, four additional test specimens were manufactured one week later. All eight specimens were tested. The four specimens brushed in wrong direction were used in pilot tests, with successive changes in the set-ups. In this report, only the tests on specimens brushed in the correct direction are described. Shear elements brushed in the correct direction, delivered from Hedareds Sand & Betong were named: **S-HR1**, **S-HR2**, **S-HR3** and **S-HR4**. The shear elements delivered from Hedareds Sand & Betong with wrong direction were named: **S-HF1**, **S-HF2**, **S-HF3** and **S-HF4**.

The shear elements delivered from Abetong were designated: **S-A1**, **SA-2**, **S-A3** and **S-A4**. The surface of the prefabricated concrete was treated with single grooves, with a distance of about 100 mm, see Figure 4.

The area where the prefabricated and in situ cast concrete were in contact (and constitute the actual cast joint) is here called shear area. The shear area of each specimen was measured after the guide notch was sawn and the tests were performed, see Table 3

Table 3 Measured shear area for each specimen

Specimen	b [mm]	h [mm]	A [mm^2]
S-HR1	110	200	22000
S-HR2	110	205	22550
S-HR3	110	204	22440
S-HR4	111	206	22866
S-A1	110	204	22440
S-A2	112	204	22848
S-A3	110	200	22000
S-A4	110	204	22440

2.3.2 Test set-up

In the shear tests, the shear capacity and behaviour of the grouted joint were tested. As mentioned earlier, four test specimens were used in pilot tests were the test set-up was worked out. In the first of these tests, load was applied on only parts of the end cross-sections. However, this led to problems with horizontal cracking. The main reason for this cracking was that the top and bottom surfaces of the specimens were not parallel enough. To reduce the problem with horizontal cracks, load was applied on the whole top surface and on the corresponding part of the bottom surface, see Figure 5. Displacement transducers were used; Nos. 1-4 measured the slip and Nos. 5-8 measured the opening of the joint. The load was controlled by the displacement in the testing machine; by a speed of 0.05 mm/min. Furthermore, the total deformation between the loading plates was also measured by a separate displacement transducer.

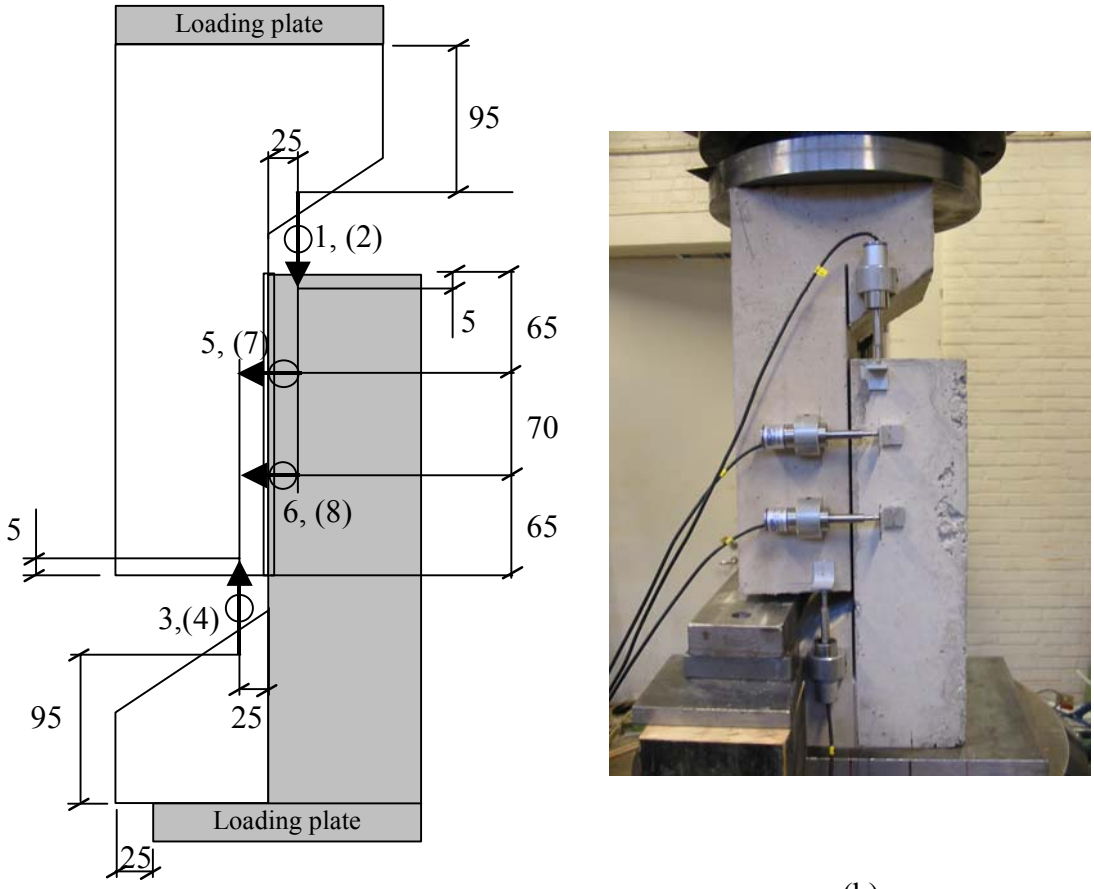

Figure 5 *(a) Set-up of shear tests with displacement transducers. Nos. 1-4 measured the slip and Nos. 5-8 measured the opening of the joint. The numbers within parentheses are displacement transducers on the backside of the specimen. (b) Photograph.*

2.4.3 Shear test results

The shear test results are presented in force versus vertical deformation relationship in Figure 6. The vertical deformation between the two parts (prefab and *in situ*) is calculated as the average of the ones measured in displacement transducers 1-4. In all tests, the failure was very brittle; it was not possible to follow any descending part as the test specimens fell apart at failure, see Figure 7a. Maximum capacities measured in the tests and corresponding bond stresses are tabulated in Table 4. When comparing the tests from Hedareds Sand & Betong and Abetong, there were higher shear capacity and less scatter in the results of the test specimens delivered from Hedareds Sand & Betong.

The four specimen delivered from Hedareds Sand & Betong (S-HR1 – S-HR4, Figure 6a) had almost the same behaviour: linear behaviour until a value about 70 kN, when unfortunately two horizontal cracks appeared, see Figure 7b. The main reason for these cracks were that the test specimens were not perfectly flat at the loading and

support surfaces; thereby the boundary conditions introduced and allowed small rotations. Due to the crack appearance the force decreased, but could then be further increased until the joint collapsed at a final value of about 100 kN. The measured vertical deformations therefore include not only slip over the joint, but also deformations in the cracks. However, the maximum loads were most likely not influenced by the cracks, as failure in all tests took place in the grouted joint.

Figure 6b show the shear test results of specimens S-A1 – SA4. In these tests, the elastic behaviour was similar in all tests, but the peak load had a quite large scatter. Failure in all tests took place in the grouted joint; the parts between the grooves were almost unaffected by the test while the *in situ* cast concrete that had protruded into the grooves were cracked. SA-1 and SA-3 deviated a lot compared to S-A2 and S-A4 and the explanation could be differences of dimensions in the grooves; larger grooves gave higher capacity. The grooves were made by hand which lead to scatters in the dimension. Only one specimen had a horizontal crack during the tests, S-A3.

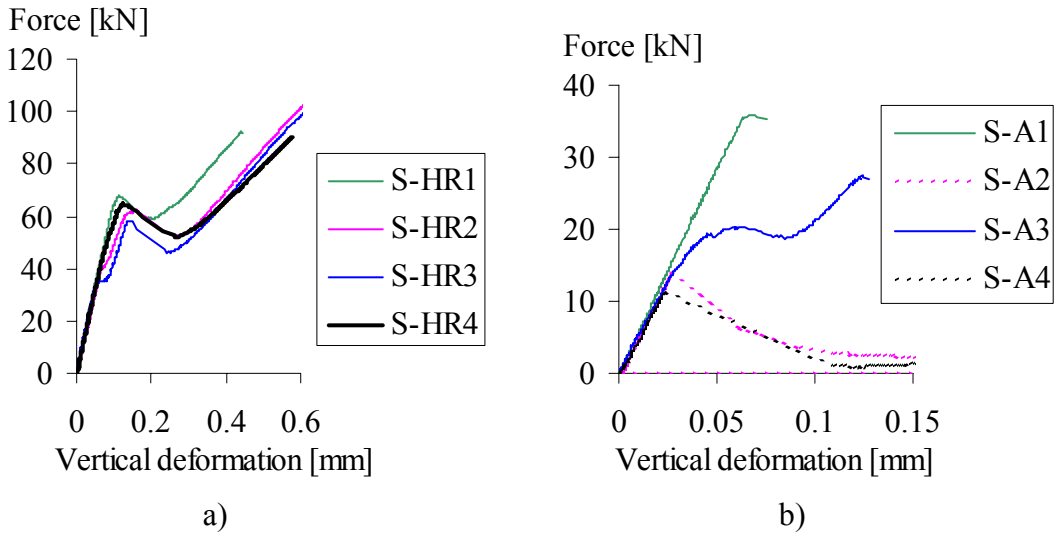

Figure 6 *Force versus vertical deformation in shear tests. a) Test specimens from Hedareds Sand & Betong, and b) Test specimens from Abetong. Dashed lines indicate that the descending parts could not be followed; however in these tests it was possible to measure deformation for small loads again. Note the different scales*

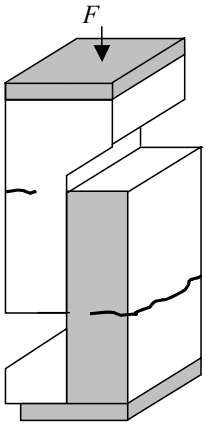

a) b)

Figure 7 *(a) Test specimen falling apart at failure, and (b) Horizontal cracks in the shear test specimens from Hedareds Sand & Betong.*

Table 4 *Measured maximum loads and corresponding shear stresses in the shear tests.*

Specimen	Maximum load [kN]	Maximum shear stress [MPa]
S-HR1	98.1	4.46
S-HR2	102.9	4.56
S-HR3	99.1	4.42
S-HR4	90.4	3.95
Average	97.6	4.35
S-A1	35.8	1.60
S-A2	14.0	0.61
S-A3	27.4	1.24
S-A4	11.4	0.51
Average	22.1	0.99

In the tests, there were also horizontal deformations between the two parts (prefab and *in situ*): normal deformations. The force versus average horizontal deformation, calculated as the average from displacement transducers 5-8, is presented in Figure 8. As can be seen, the horizontal deformations increased just before peak. The normal deformations increase more before peak than the vertical deformations did, as can be seen in Figure 9. The results from test specimens from both suppliers are compared for small slips in Figure 9c; as can be seen, the normal deformations were of the same size. The variation in measurements of both vertical and horizontal deformations was rather small, see Figure 10 for an example and Appendix B for all test results.

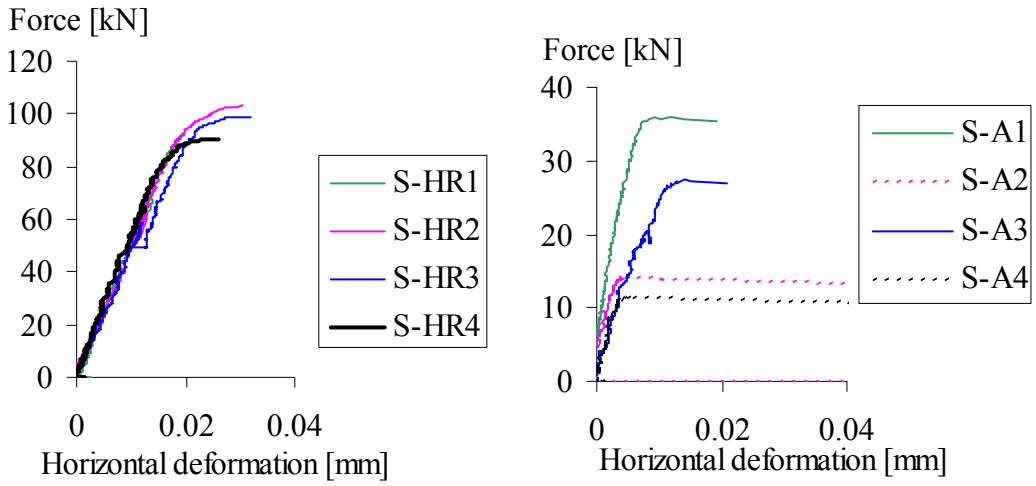

Figure 8 *Force versus horizontal deformations. a) Test specimens from Hedareds Sand & Betong, and b) Test specimens from Abetong. Note the different scales.*

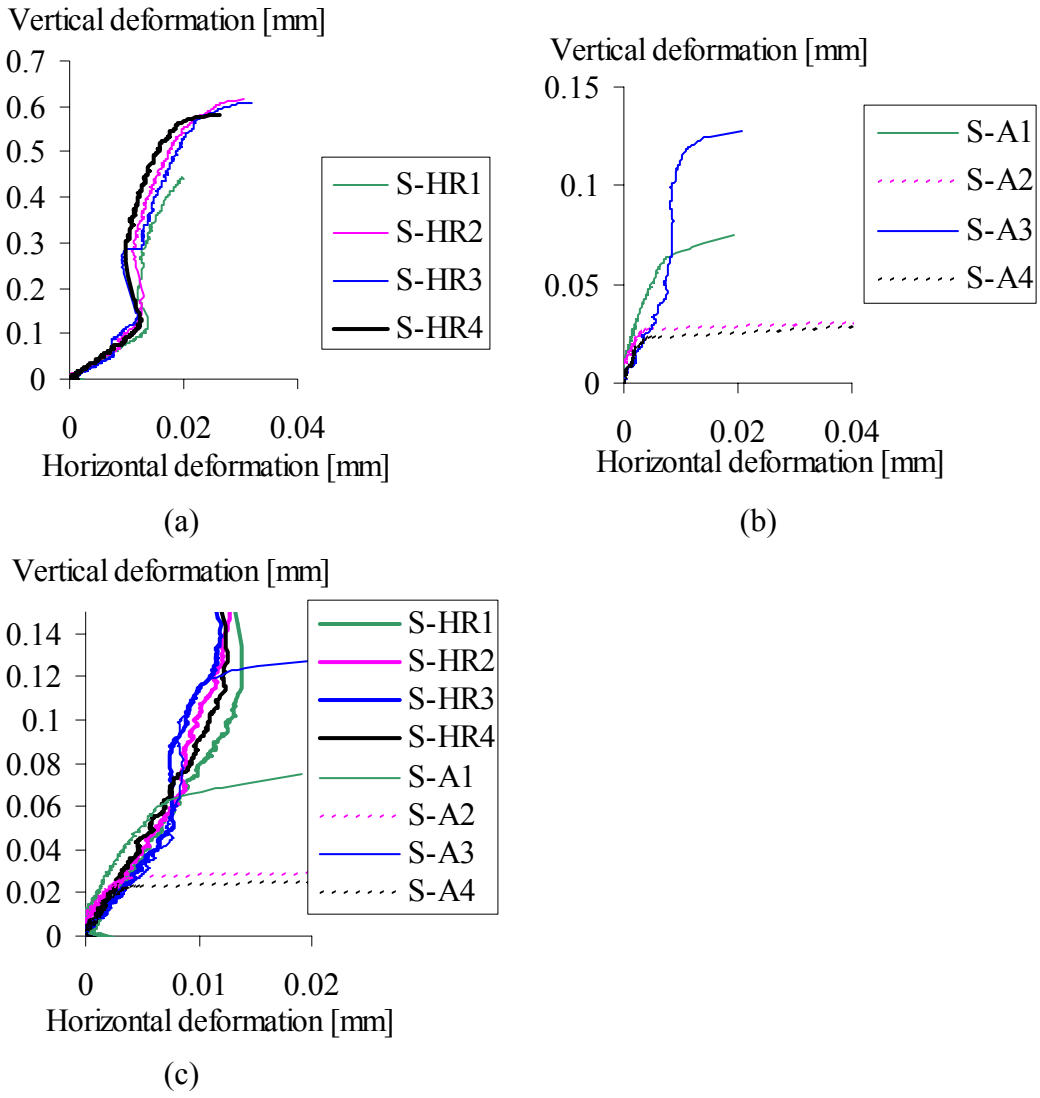

Figure 9 *Vertical versus horizontal deformations. a) Test specimens from Hedareds Sand & Betong, b) Test specimens from Abetong, and c) Comparison of all shear tests.*

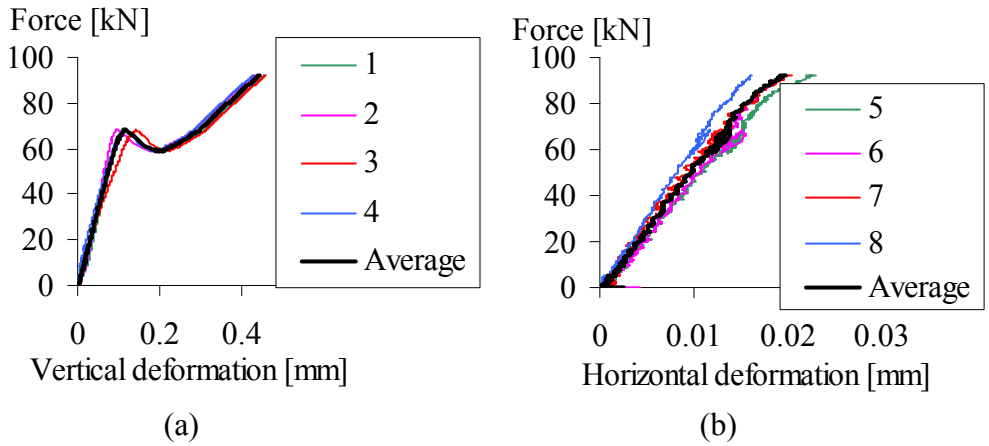

Figure 10 *Example of scatter in measurements of a) vertical and b) horizontal deformations. From test no. S-HR1.*

2.4 Wedge split tests

2.4.1 Test specimens

The wedge split components were delivered in total of eight, four from each company. Similar as the shear test specimens, the geometry of the wedge split test specimens was the same from both suppliers, while the treatment of the surfaces differed. The test specimens consisted principally of 200*200*150 mm^3 cubes, where half of the specimens were of prefabricated and half of *in situ* cast concrete, see Figure 11. No reinforcement was placed in the wedge split components. A guide notch was sawn with a width of 4 mm and a depth of 78 mm.

The wedge split test specimens delivered from Abetong were named: **W-A1**, **W-A2**, **W-A3** and **W-A4**. The treatment of the surfaces was also here performed with single grooves, see Figure 11c. The wedge split test specimens delivered from Hedareds Sand & Betong were named: **W-H1**, **W-H2**, **W-H3** and **W-H4**. They had brushed surfaces, as shown in Figure 11d.

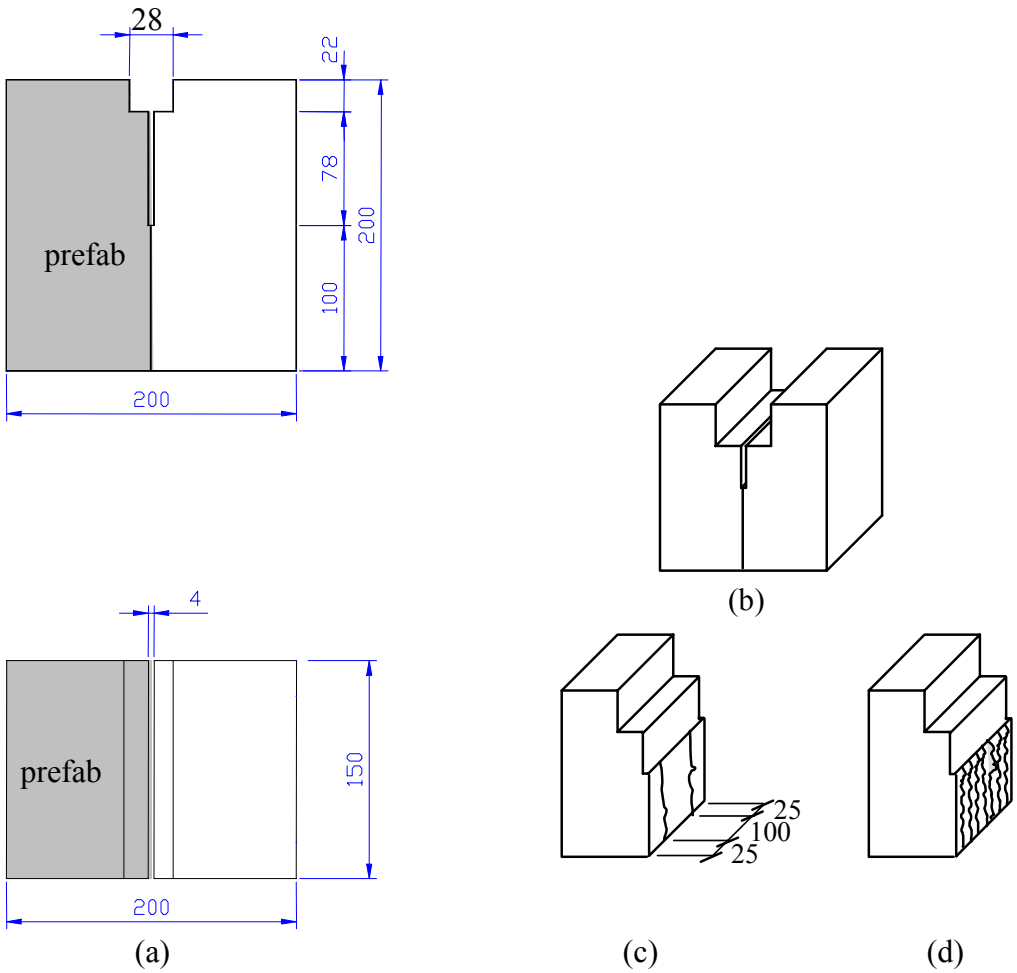

Figure 11 *Wedge split elements geometry. a) Measurements, b) Three-dimensional sketch, c) Surface treatment of specimen from A-betong, and d) Surface treatment of specimen from Hedared.*

2.4.2 Test set-up

The wedge split test (WST) was formerly developed in purpose of measuring fracture energy (G_F) for homogenous concrete. It was proposed by Linsbauer and Tschegg (1986), and has proven to be a reliable test method. In this project, the wedge split test was used to increase the knowledge of the joint behaviour for tensile loading. From the WST, the tensile strength and fracture energy of the joint could be evaluated. A schematic procedure of test set-up and equipment are shown in Figure 12. To be able to apply a vertical force the test specimens were designed with a notch and to ensure vertical crack propagation in the joint, a guide notch was also sawn, see also Figure 11. A roller made of steel acting as a roller support, allowing rotation, supported the wedge test specimens.

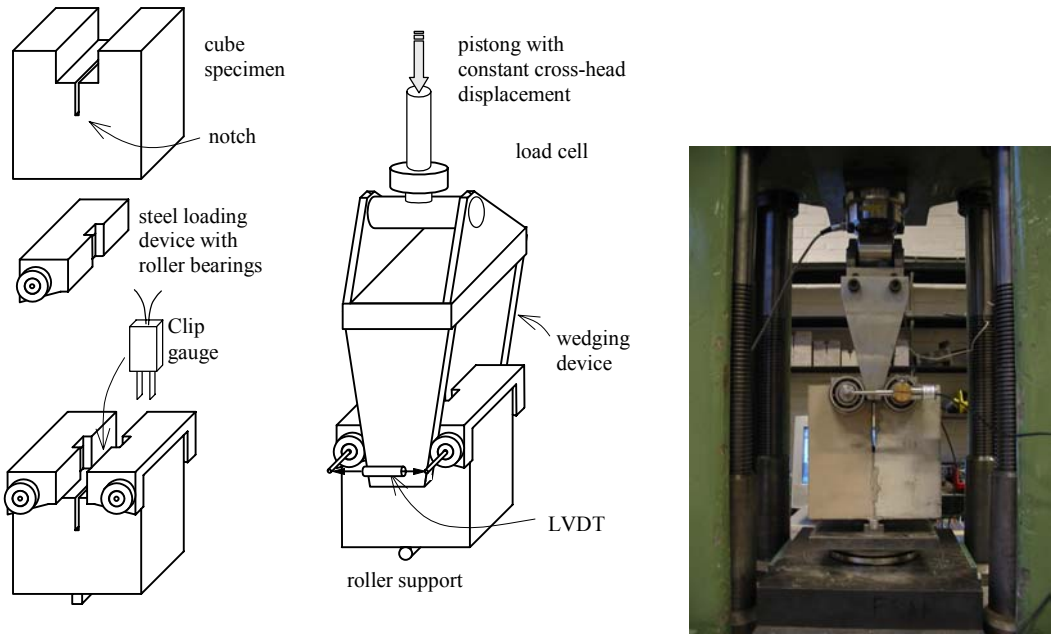

Figure 12 Schematic view of test equipment and test set-up, b) Photograph of specimen and equipment

On top of the wedge test specimens, two steel plates with roller bearings were placed. Through a wedging device, the splitting force was applied. Throughout the tests the vertical load F_v and the crack mouth opening displacement (CMOD) and the horizontal displacement were measured at the same level as the load was applied.

The applied horizontal splitting force F_{sp} is related to the vertical load and was calculated according to:

$$F_{sp} = \frac{F_v}{2 \times \tan(\alpha)} \times \frac{1 - \mu \times \tan(\alpha)}{1 + \mu \times \cot(\alpha)} \Rightarrow F_{sp} = \frac{F_v}{2 \times \tan(\alpha)} \quad (1)$$

where α is the wedge angle, and μ is the coefficient of friction for the roller bearing. Wedge angle $\alpha = 15°$ was used in these tests. The coefficient of friction was in this

case assumed to be negligible; according to Karihaloo (1995) it normally varies between 0.1% and 0.5%.

The tests were performed in a deformation controlled test machine. The rate of vertical displacement was approximately 0.06 mm/min, which resulted in a CMOD-rate of approximately 30 μmm/min. How the forces F_v and F_{sp} were applied through the wedge split device and the roller bearings is shown in Figure 13.

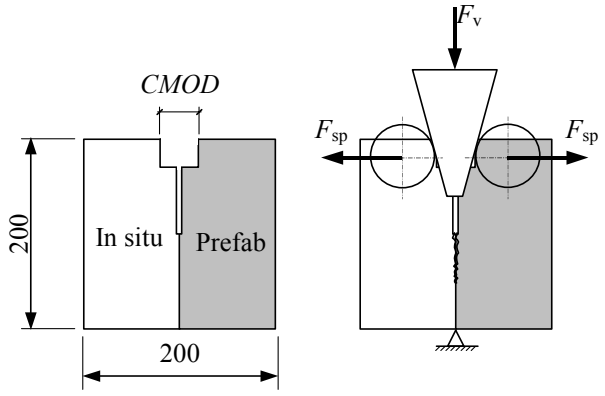

Figure 13 Sketch of WST, CMOD and applied forces F_v and F_{sp}

2.4.3 Wedge split test results

The behaviour of the WST was similar between the two manufactures. The difference was the maximum vertical load (F_v), which was about twice as high for Hedareds Sand & Betong than for Abetong, see Figure 14. After cracking there was a very fast decrease of the load, which unfortunately could not be followed by the machine; this is indicated as dashed lines in Figure 14. Thus, the decrease of load should be much more brittle than indicated by the dashed line in Figure 14. Tests W-H1 and W-A1 both differ from the other tests. During W-H1 there were problems with the displacement transducer and in W-A1 the loading plate had an odd angle.

All cracks were perfectly formed in the joint. Figure 15 shows the joint in W-A3. When the crack was initiated it was small and difficult to see. The CMOD increased during the tests and was visible in the end stage.

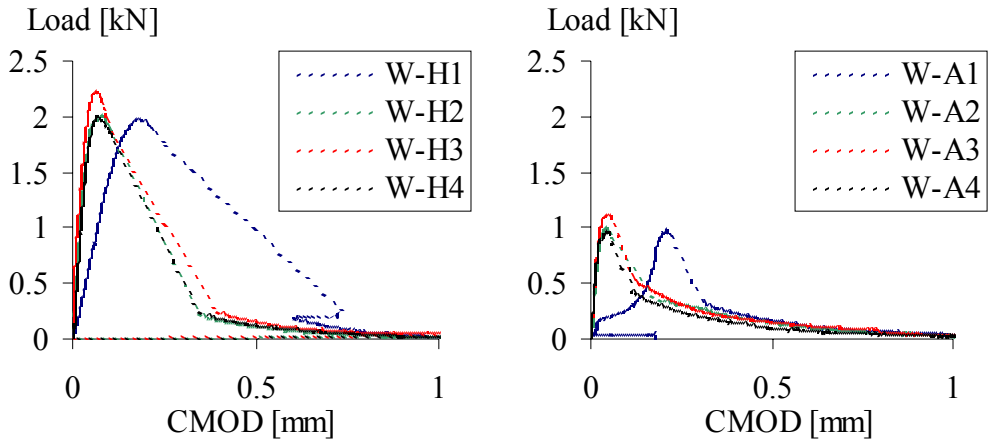

Figure 14 *Vertical load versus CMOD, a) Hedared and b) Abetong.*

Figure 15 *The joint in test W-A3 after testing.*

2.5 Full-scale tests

2.5.1 Test specimens

The geometry of the full-scale tests was lattice girders composed of two precast elements next to each other, with a reinforcement mesh placed directly on the surface over the joint. Concrete was cast *in situ* on top, see Figure 16. The test specimens had a total width of 500 mm in the plane, and the placement of the reinforcement mesh in the prefabricated part was as shown in Figure 17.

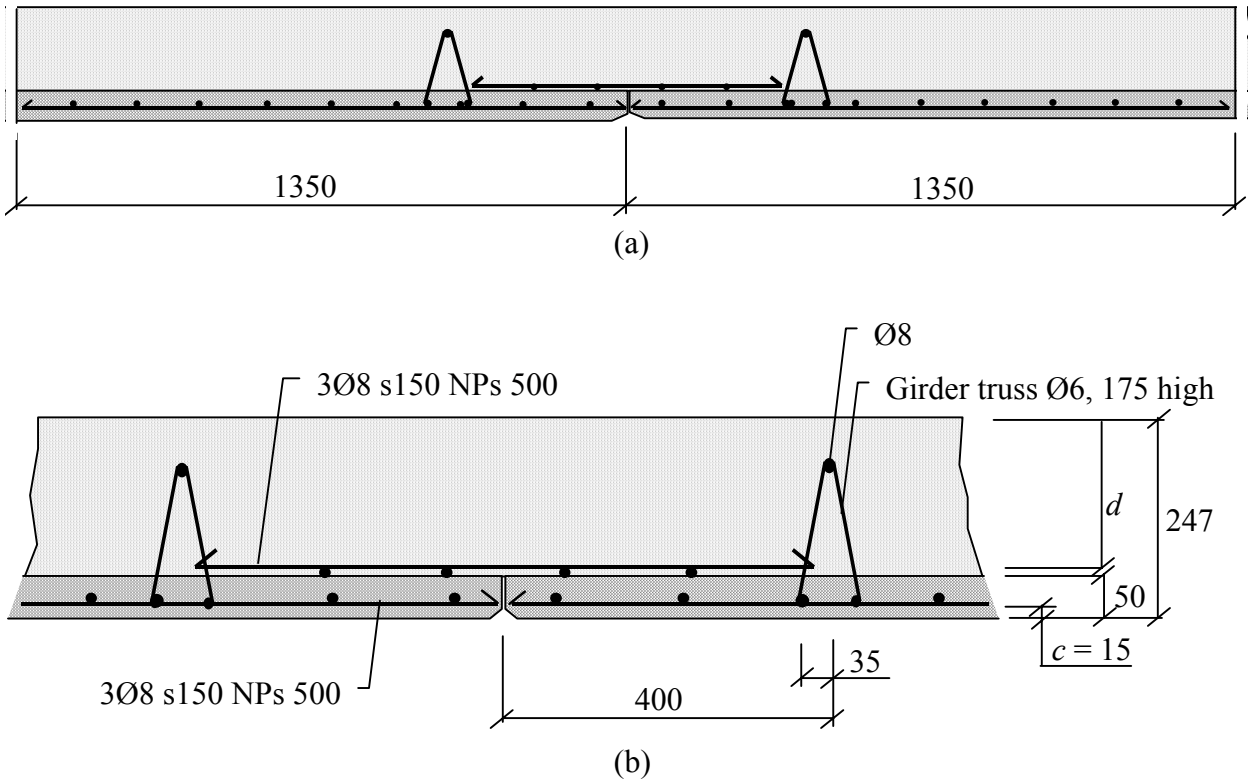

Figure 16 Geometry of the lattice girder structure, a) Overview, and b) Detail at the joint.

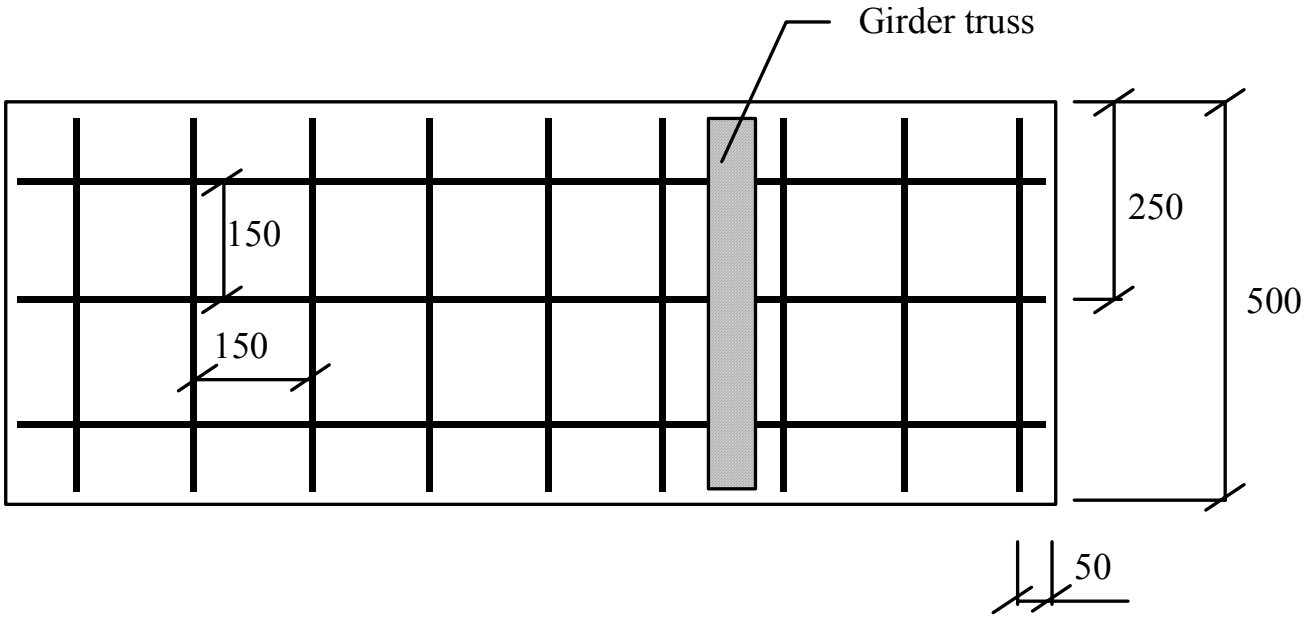

Figure 17 Placement of reinforcement mesh in prefabricated parts.

The prefabricated elements delivered from Hedareds Sand & Betong had a brushed roughened surface between the lattice girder trusses. The direction of the brushed

surface was in the towards the lattice girder trusses; *i.e*. perpendicular to the ordinary main load-carrying direction. The prefabricated elements delivered from Abetong had single grooves in the surface between the lattice girder trusses; parallel to the lattice girder trusses. The grooves were meant to be with a distance of approximately 100 mm from each other, However, in all test specimens except one (one of the prefabricated parts in test A2), there were 5 grooves on 400 mm distance; i.e. the grooves were slightly closer than 100 mm from each other. Examples of surfaces are shown in Figure 18.

Figure 18 *Examples of surfaces of the prefabricated components in the full-scale tests: a) Hedared, and b) Abetong.*

Each supplier delivered 6 prefab components, which were put together two and two, thus in total 6 full-scale test specimens were made. Elements delivered from Hedareds Sand & Betong were named: **H1**, **H2** and **H3**. Elements from Abetong were named: **A1**, **A2** and **A3**. One important input in the numerical analyses, is the distance d between the reinforcement mesh and top of the *in situ* concrete layer, see Figure 16. This distance was measured before *in situ* casting was made, and also after the tests, see Table 5. The measurement after the tests corresponds better to reality, as it was rather easy to measure when the test specimen were divide in two parts. The measurements made before the *in situ* casting included a small uncertainty of where the upper level of concrete would be. The values of *d* measured after the tests were larger for all cases. This is due to that the concrete pushed down the reinforcement, and the height of the beam had increased from 247 to 250 mm.

Table 5 Measured distance d between centre of reinforcement bar and top of in situ concrete layer

	Bar	1	2	3	Average
H1	$d_{bef.}$ [mm]	178	175	174	176
	d_{after} [mm]	180	180	175	**178**
H2	$d_{bef.}$ [mm]	178	176	176	177
	d_{after} [mm]	185	186	182	**184**
H3	$d_{bef.}$ [mm]	176	175	176	176
	d_{after} [mm]	180	181	179	**180**
A1	$d_{bef.}$ [mm]	178	176	179	178
	d_{after} [mm]	189	186	185	**187**
A2	$d_{bef.}$ [mm]	176	176	175	176
	d_{after} [mm]	185	185	182	**184**
A3	$d_{bef.}$ [mm]	177	179	178	178
	d_{after} [mm]	185	185	186	**185**

2.5.2 Test set-up

The full-scale tests were performed to study the structural behaviour of the joint in the lattice girder structure. The test specimens were loaded by two point loads (P) in four-point bending, see Figure 19. This loading was chosen to achieve a constant bending moment at the weak section. The point loads were applied on steel beams (HEA 160), to achieve a line load through the total depth in the plane. Two hydraulic jacks were connected to the same hydraulic pump, which leads to equal load of the two point loads. The tests were provided with ten displacement transducers to measure the vertical displacement. The displacement transducers were placed in two rows, 100 mm from the edges of the specimens.

Loading was applied with displacement control; steering displacement was an extra displacement transducer in the centre of the specimen. The rate of vertical displacement was approximately 0.1 mm/min until yielding of reinforcement; thereafter the rate was increased to 0.4 mm/min. During the tests all data were stored in a computer. In addition, a load deflection relationship was plotted to be able to observe the behaviour of the structure during the tests. The plotted load deflection

relationship was measured by one of the point loads (P) and the extra displacement transducer located in the centre of the structure.

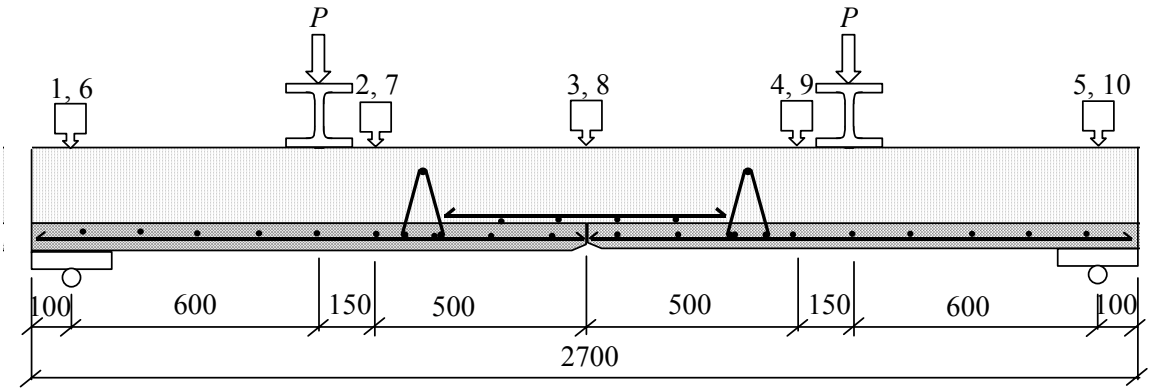

Figure 19 Test set-up with displacement transducers and loads

To be able to measure the strains in the reinforcement across the joint, strain gauges were placed on the centre bars of the reinforcement meshes. The number of strain gauges were nine in each test; Figure 20 shows the strain gauges arrangement.

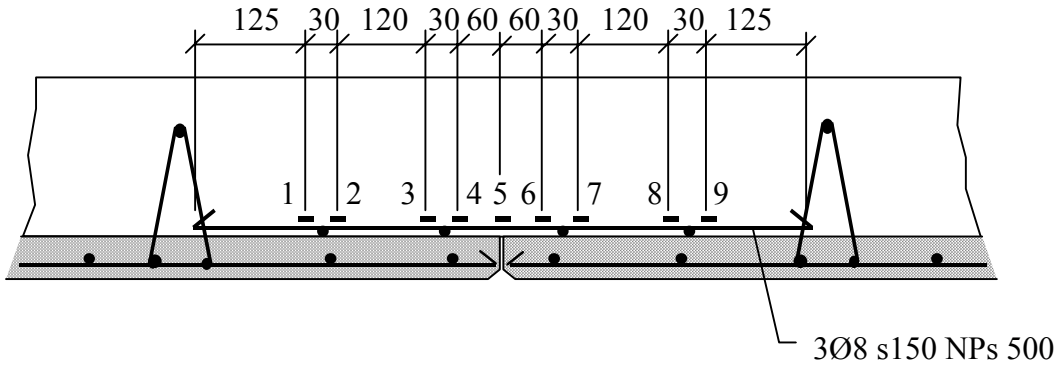

Figure 20 Arrangement of strain gauges, on the centre reinforcement bar

2.5.3 Full-scale test results

The structural behaviour was similar for all six full-scale tests, with only one crack in all tests, at mid span in the *in situ* cast concrete over the joint. Rupture of the reinforcement bars as failure mode in all tests.

A typical load versus deformation plot is shown in Figure 21. The structural behaviour corresponded to linear elastic response until a load of about 11 kN. Instantly, the first crack appeared and the load made a small dip, see Figure 21 and Figure 22a for crack pattern. Thereafter, the concrete showed non-linear material behaviour and the reinforcement carried the tensile stresses and had linear elastic response until yielding. The load and deflection increased to the value of

approximately 18-20 kN (P_{yield}) and 1.6-1.9 mm respectively. At this load yielding of the reinforcement occurred and the initiated crack propagated in the same direction as it started, see Figure 22. At yielding stage the load remained almost constant, besides a very small increase of load due to hardening of the steel. Semi-collapse occurred when one of the longitudinal bars ruptured at the load $P_{1stcoll}$, approximately at 20 kN and the deflection about 18-21 mm. The remaining longitudinal bars provided further load-carrying capacity under a decreasing load until $P_{2ndcoll}$ was reached of about 20 kN. Total collapse of the structure occurred at a deflection of about 28-33 mm.

The load versus deflection from all six tests is compared in Figure 23. The deflection is corrected for the measured support settlements. In tests H1 and H2, there were disturbances from the hydraulic pump. In test H2, an unloading occurred; this was also because the problem with the hydraulic pump. The first crack appeared at almost the same point in the graph; which is reasonable as the crack was formed in the *in situ* cast concrete. The start point for yielding of the steel differs more, which is due to that the distance from top of the *in situ* concrete to the reinforcement, d, determines the yield start point, and it differed some between the different test specimens, see Table 5. It can be noted that test H1 with the smallest value of d also had the lowest yield load, while test A1 had the largest yield load and largest d. The joint between the prefab concrete and the *in situ* concrete didn't show any visual movement or opening.

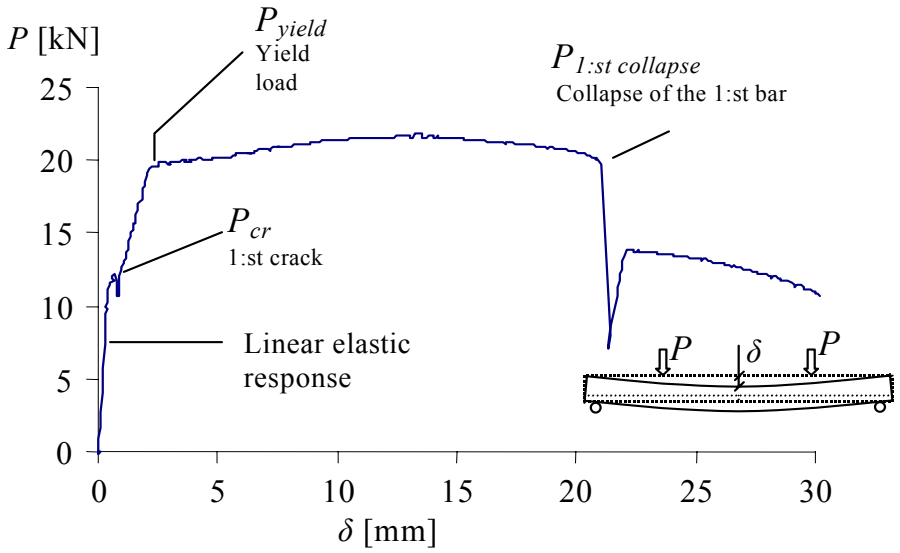

Figure 21 General load versus deflection and behaviour of the full-scale tests.

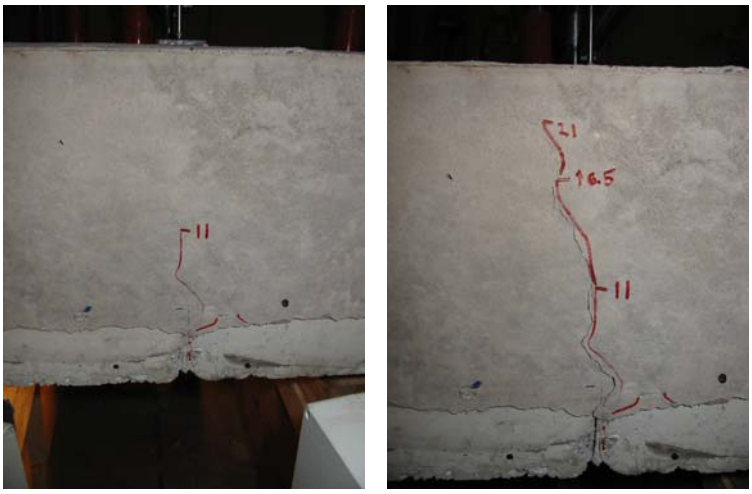

(a) (b)

(c)

Figure 22 *a) First crack for a load of P = 11 kN. b) The initiated crack propagated and yield load was reached. c) Test specimen after collapse.*

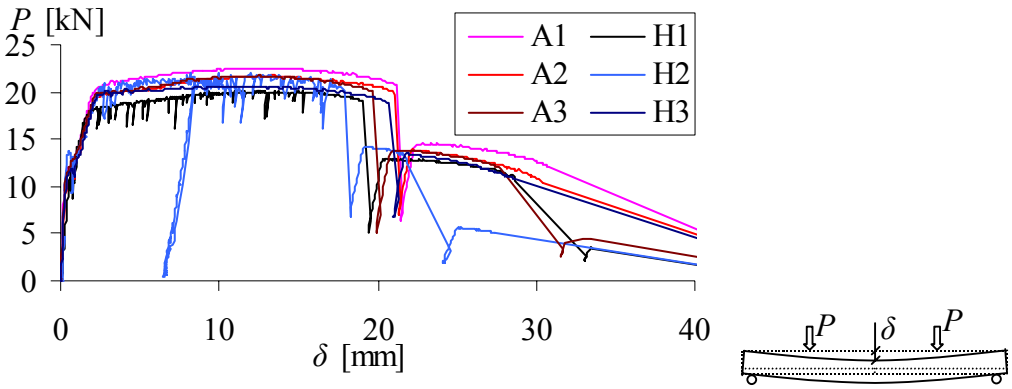

(a)

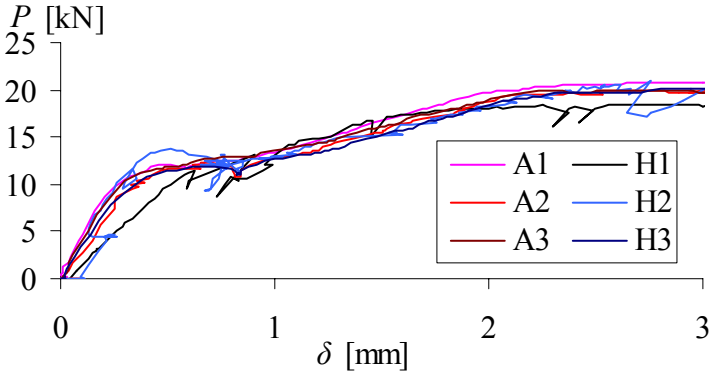

(b)

Figure 23 *Load versus deflection for all six full-scale tests. Deflection is corrected for support settlements. a) Full plot, and b) First part enlarged.*

Measured load and deflection at the interesting points, such as crack stage, when yielding occurred and when collapse took place differed slightly between the tests are tabulated in Table 6.

Table 6 *Measured load and mid-span deflection corrected for support settlements at certain points.*

Test	H1	H2	H3	A1	A2	A3
P_{cr} [kN]	11.5	13.0	12.0	12.0	12.3	11.5
δ_{cr} [mm]	0.627	0.763	0.705	0.458	0.700	0.442
P_{yield} [kN]	16.0	17.0	17.8	18.8	17.0	17.8
δ_{yield} [mm]	1.486	1.735	1.987	1.818	1.694	1.641
$P_{1stcoll}$ [kN]	19.0	20.2	18.8	20.7	19.7	19.9
$\delta_{1stcoll}$ [mm]	19.09	17.90	20.34	21.18	21.05	19.33
$P_{2ndcoll}$ [kN]	10.7	12.5	10.7	12.0	10.5	11.9
$\delta_{2ndcoll}$ [mm]	28.67	21.89	28.21	30.83	30.39	27.18
$P_{3rdcoll}$ [kN]	3.4	5.0	-	-	-	4.5
$\delta_{3rdcoll}$ [mm]	33.54	27.34	-	-	-	32.19

The measured strain during the test is presented in Figure 24 for A2, the strain measured in the other tests were similar, see Appendix C. The plots in Figure 24 represent the variation of strain along the reinforcement bar for a specific load case. As can be seen, the strain reached the highest value in the mid-section for all load cases. This was expected due to the crack localisation in the mid-section. With increasing distance from the mid-section the measured strain value decreased and at only 200 mm away from the centre, the strain was almost zero. The transverse cross-bars in the reinforcement mesh contributed only little to the anchorage; as there were only small increase in strains between the measurements made on each side of the cross-bars. One reason for this can be that the reinforcement mesh was put directly on the surface of the prefabricated concrete without any distance between the cross-bars and the grouted concrete. Therefore, the cross-bars were most likely not very well-confined. However, the reinforcement bars in the mesh that in these tests carried the stresses were obviously confined enough to obtain a good bond to the concrete, as the increase in strains between the cross-bars was high.

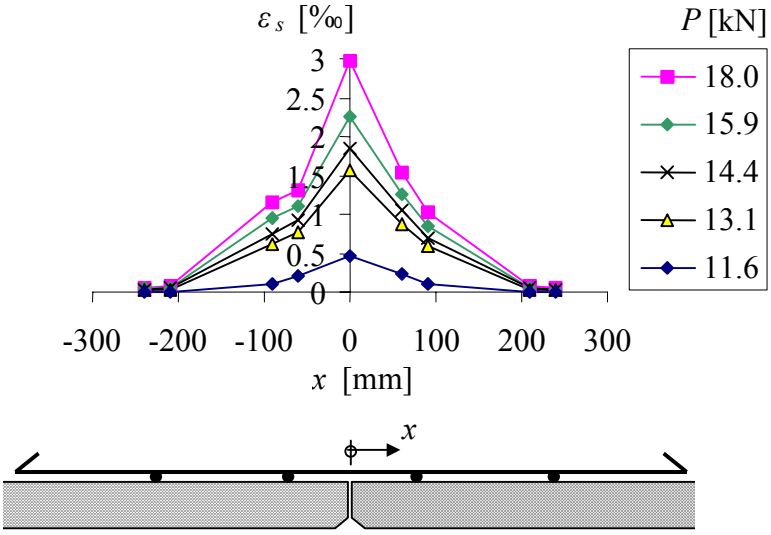

Figure 24 *Measured steel stress in the reinforcement bar in the centre at various load levels. From test No. A2.*

3 Finite Element Modelling

Non-linear finite element analyses were used to model the tests. The programme DIANA 8.1.2 was used in all analyses.

3.1 General modelling

As described in Chapter 2, three different types of tests were performed; they were all modelled by finite element analyses. All modelling were made in two dimensions, assuming plane stress. The geometry of the models can be seen in chapter 3.2, 3.3 and 3.4. The parts that are the same in these models are described here. The concrete was modelled with four-node quadrilateral isoparametric plane stress element. The cast joint was modelled with interface elements, with separate nodes for the precast and the *in situ* cast concrete, see Figure 25.

Simplifications made in the models were that long-term effects such as creep and shrinkage were not included. These would have some influences when the joint is subjected to sustained tensile loading. These simplifications need further studies.

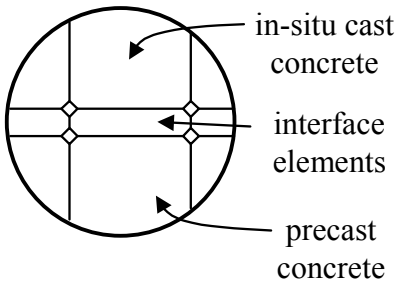

Figure 25 Modelling with two-dimensional solid elements describing the concrete and interface elements describing the cast joint.

3.2 Model of shear test

The mesh and boundary conditions of the shear test model are shown in Figure 26. The mesh size was 10 mm; the thickness out of plane of the concrete elements was 200 mm and of the cast joint layer 110 mm. Friction layers were modelled at the support and loading plates. The modelled test specimen was not supported in any direction; while the nodes representing the loading plates were tied in all directions. Loading was controlled by applying a vertical displacement on the nodes at the top representing the loading plate. Chosen input data for the friction layers at the support and loading plates are shown in Table 7. The joint between the different concrete types is further described in section 3.6.

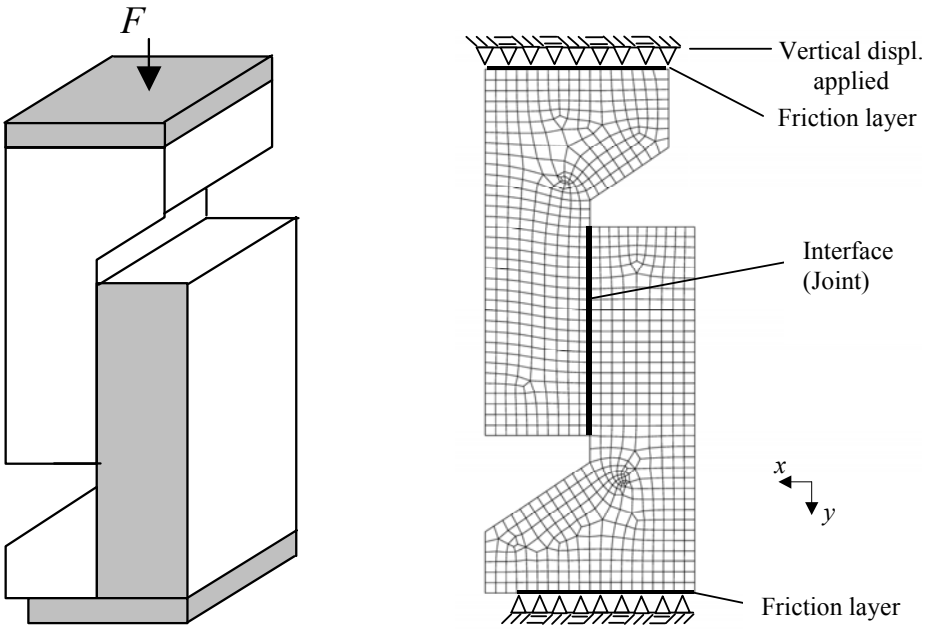

Figure 26 *a) Principle sketch of shear test. b) Finite element model.*

Table 7 *Input data for the friction layers at the support and loading plates in the shear test model.*

μ [-]	η [-]	D_{11} [N/m^3]	D_{22} [N/m^3]	f_{a1} [MPa]
0.4	0.1	$1 \cdot 10^{11}$	$1 \cdot 10^{11}$	0

3.3 Model of wedge split test

The geometry of the wedge split test was modelled as shown in Figure 27, with mesh size of 8 mm. Loading was applied by load control. The analysis must be stable through the whole analysis process, from start until collapse. This was achieved by crack mouth opening displacement (CMOD) with arc-length control, see TNO (2002). The minimum step size had to be small in the FEA to give convergence in as many steps as possible. The support in the bottom of the WST had a width of 20 mm and was modelled by locking respective nodes in *y*-direction and the two nodes in centre locked in *x*-direction. Interface elements were used to model the joint between the precast and *in situ* cast concrete.

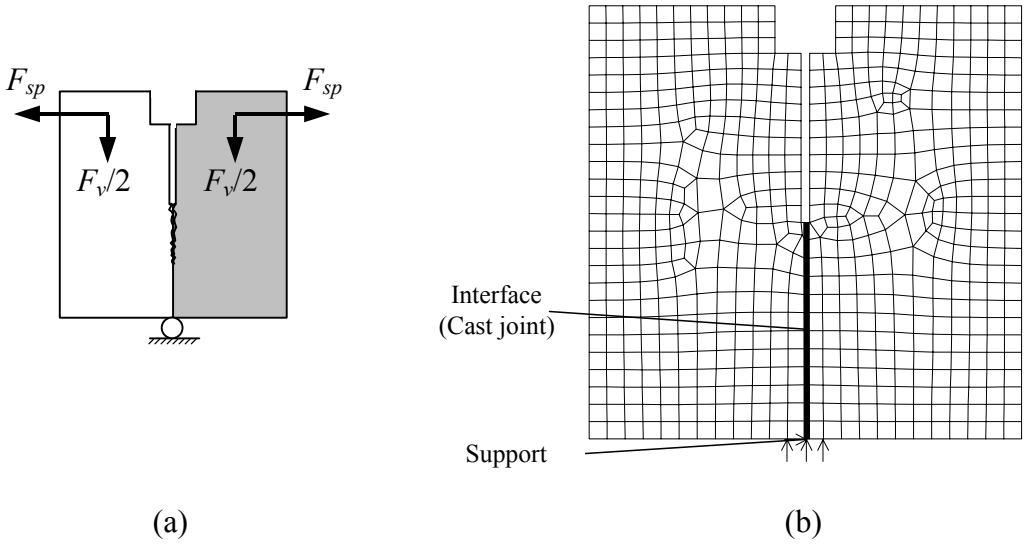

Figure 27 a) Principle sketch of wedge split test. b) Finite element model.

3.4 Model of full-scale test

3.4.1 Overview of model

In the model of the full-scale tests, some simplifications were made to decrease the number of elements and in that way speed up the analyses. The simplification was to model the right part from the right lattice girder truss with only beam elements, see Figure 28. The left part was modelled in detail, with the cast joint modelled with interface elements. The reason for this choice (i.e. not to use symmetry) was because in an experiment, the structure would not be symmetric if failure was determined by opening of the cast joint.

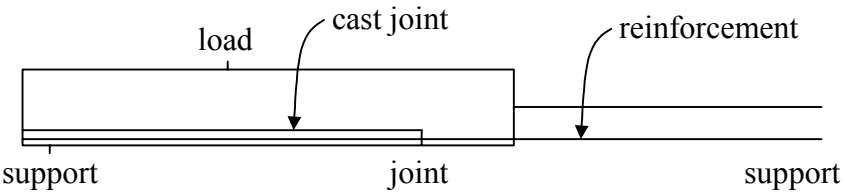

Figure 28 Geometry of model with detailed modelling of the left part and the right part simplified modelled with beam elements.

In Figure 29, a detail over the connection between the prefabricated elements and the cast joint is shown.

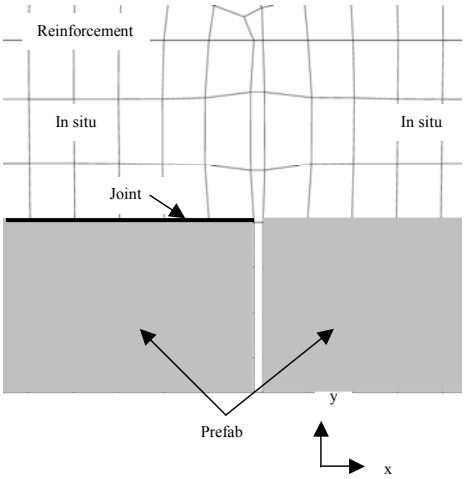

Figure 29 Detail of the modelling of the prefabricated and in situ cast concrete and the cast joint

To be able to run the analysis in deformation control, one had to model an external beam. This beam was tied to the loading plates on the lattice girder. The deformation was applied in the centre of the external beam, which leads to equal load on the two loading plates, see Figure 30.

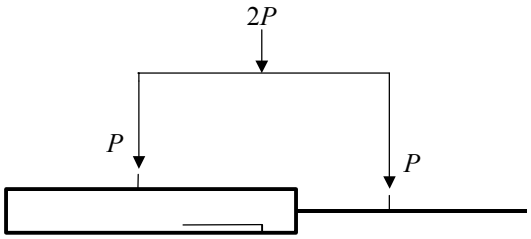

Figure 30 External loading beam: by applying a deformation in the centre, equal forces P were obtained at the lattice girder structure.

3.4.2 Reinforcement

The reinforcement in the left part was modelled with truss elements. Special interface elements were used between the reinforcement and the concrete, describing a bond-slip relation. The relation was chosen according to CEB (1993), assuming unconfined concrete and other bond conditions; see Figure 31. The welds in the reinforcement mesh were modelled with the reinforcement and the concrete nodes tied to each other at the points of the welds, see Figure 32. The distance *d* between the reinforcement mesh and top of the *in situ* concrete layer was 177 mm in the FEA. This can be compared with the average in the tests, which was 183 mm (see Table 5). The reason for the difference was that the total thickness of the slab became slightly larger than intended in the tests, 250 mm instead of 247 mm, and that the weight of the concrete pushed down the reinforcement at grouting. The lattice girder truss was modelled by tying the *in situ* and precast nodes to each other in the centre of the truss. This is a

simplification while the real behaviour is that the truss only limits the joint from opening at the points where the truss crosses the joint.

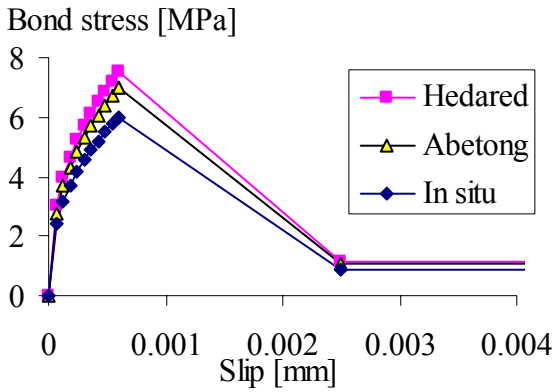

Figure 31 *Bond versus slip correlation used as input for the interaction between the concrete and the reinforcement*

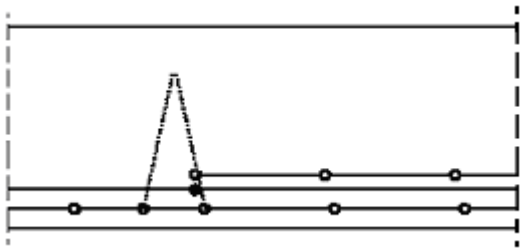

Figure 32 *Part of the model. White circles mark where the concrete and reinforcement nodes were tied to each other. The filled circle mark where the nodes of the precast concrete and the in situ concrete were tied to each other.*

The reinforcement in the beam part was modelled as embedded reinforcement; there perfect bond was assumed and bond slip was not included.

The constitutive behaviour of the reinforcement was modelled by the Von Mises yield criterion with associated flow and isotropic hardening. The stress-strain relationship used corresponded to the measured force versus strain in the tensile tests of the reinforcement (Figure 3). By using the nominal area of the reinforcement bar, a stress-strain relationship as shown in Figure 33 was obtained. The elastic modulus of the reinforcement was 189 GPa and first yielding occurred at a stress of 438 MPa. These values can be considered to be rather small for the steel; the main reason is that in reality the diameter of the reinforcement bars was slightly smaller than nominal 8 mm. However, as the nominal diameter was used in the analyses, the stresses should correspond to that.

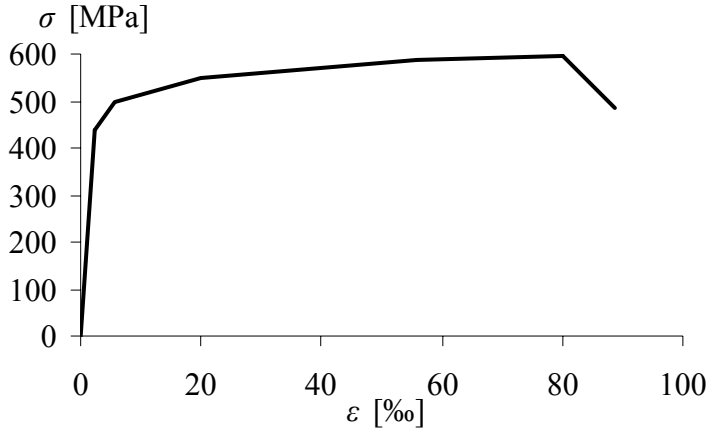

Figure 33 Stress-strain relationship of reinforcement used in FEA.

3.4.3 Boundaries

At the supports with roller bearings, steel plates were used in the tests. In the part modelled in detail, the steel plate was modelled such that the nodes representing the plate were tied to the centre node by a command called ECCENT. A dummy beam was connected to the centre node to make this possible. The centre node was supported for displacement in *x*- and *y*-direction. The same procedure was used to generate the loading plates on the top of the beam. On the right part with beam elements it was easier to model the support and loading plates while only one node in the centre of the plate was supported in *y*-direction respectively loaded. This was possible as the beam elements can not describe local crushing.

3.5 Concrete

The concrete was modelled with a constitutive model based on a non-linear fracture mechanics. As a quasi-brittle material, tensile cracking and compressive crushing characterize its response. The smeared crack concept was used, together with a rotating crack model based on total strain; see TNO (2002). The deformation of one crack was smeared out over one element in the detailed part. In the beam part a crack band width of 150 mm was chosen, corresponding to an estimated crack distance.

The compressive strength measured in cylinder tests, see section 2.2, were used as input data in the analyses. The full-scale tests were carried out first, and thereafter, after some time delay, the shear and wedge split tests. Material tests were done before and after all other tests were completed. The values measured before the other tests were used in the analyses of the full-scale tests, while the values measured after the other tests were used in the analyses of the shear and wedge split tests. From the measured compressive strengths, Young's modulus, tensile strength and fracture energy were calculated according to CEB (1993). The values used in the analyses are shown in Table 8.

Table 8 Material data of the concrete used in the analyses.

Analysis of test	Concrete	f_{cc} [MPa]	E_c [GPa]	f_{ct} [MPa]	G_F [N/m]
Full-scale tests	Abetong	48.7	36.5	3.55	90.9
	Hedared	56.7	38.4	4.00	90.5
	in situ	36.0	33.0	2.77	73.5
Shear and wedge split tests	Abetong	51.4	37.2	3.70	94.4
	Hedared	60.1	39.2	4.18	94.3
	in situ	40.8	34.4	3.07	80.3

3.6 The joint between precast and *in situ* cast concrete

3.6.1 Material model

The modelling of the joint interaction between the precast and the *in situ* cast concrete was of large importance for the results of the analyses. A friction model including adhesion was used, where the shear stresses, τ, are limited in relation to the normal stresses, σ_n, as

$$|\tau| + \mu \cdot (\sigma_n - f_a) = 0\,, \tag{2}$$

where τ is the shear stress,
μ is the coefficient of friction,
σ_n is the normal stress acting on the interface, here defined as negative when in compression, and
f_a is the adhesive strength.

The friction model is shown in Figure 34. The coefficient of friction, μ, was assumed to be constant, while the adhesive strength, f_a, was assumed to decrease at hardening. The hardening parameter κ was defined from the resulting plastic deformations as

$$\dot{\kappa} = \sqrt{\dot{u}_n^{p\,2} + \dot{u}_t^{p\,2}}\,. \tag{3}$$

Important parameters in this model are the adhesive strength, f_a, and coefficient of friction, μ. Other parameters needed were dilation parameter η and elastic stiffness D_{11} and D_{22}. The dilation parameter η, describes how large normal stresses that are created during slip if normal deformation are prevented, or how large normal deformations that will take place during slip if no normal stress is present. The stiffnesses D_{11} and D_{22} describes the relation between the stresses and the deformations in the elastic range; D_{11} for the stress and the deformation in the normal direction, and D_{22} for the shear stress and slip. The adhesive strength f_a was evaluated

and calibrated by the results from the WST. Thereafter, the coefficient of friction was evaluated and calibrated by the shear test results.

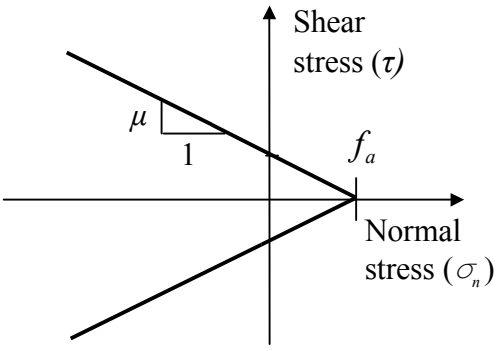

Figure 34 Friction model used for the interface between the precast and the in situ cast concrete

3.6.2 Calibration

Initially, all calibrations were made on average values of the experimental results. However, the test specimens from Abetong showed a large scatter in the shear test results; therefore two differently calibrated models were used for the analyses of the tests of Abetong's test specimens. They were denoted Abetong case 1, which used average values of the strength, and Abetong case 2 which used maximum values of the strength. The results from the WST were organized and studied with inverse analyses, see Østergaard (2003). Input to the inverse analyses were split load (F_{sp}) and the CMOD from the test results.

The inverse analysis gave a bilinear relationship between the opening of the joint, w, and the adhesive strength, f_a. As the shear stresses and deformations could be assumed to be negligible in the WST, only normal stresses and deformations took place. Therefore, the opening w is approximately equal to the hardening parameter κ; thus, the hardening function for the adhesive strength, $f_a(\kappa)$, could be evaluated. This was used as starting values for the input for the FEA, and was later calibrated to more exact values. The fracture energy of the joint, G_F, was determined as the area under the bilinear $(\sigma\text{-}w)$ plot, see Figure 35.

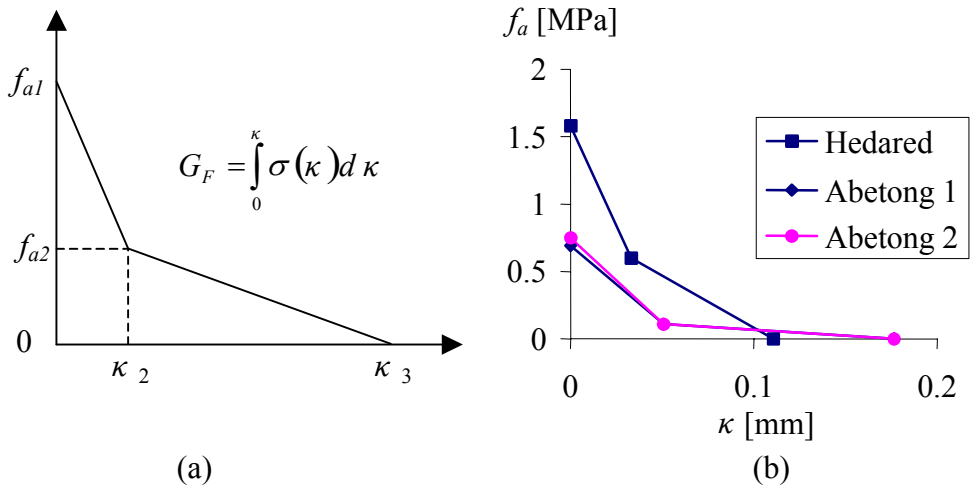

Figure 35 *a) Principal adhesive strength versus crack opening bilinear relationship, and b) Calibrated values of adhesive strength versus hardening parameter for Hedared, Abetong 1 and Abetong 2.*

The elastic stiffness D_{11} must be chosen so large that the elastic normal deformations in the wedge split tests are very small. It was chosen to $3 \cdot 10^{11}$ N/m^3 for both Hedared and Abetong.

The shear test results were carefully examined. An approximate maximum shear stress (τ_{max}) was determined through the value of the peak load divided by the shear area, see Table 4. There was no certainty that the measured shear area was in full contact at the peak load, which leads to the approximate value of the shear stress. From the WST calibration a value of f_a at max was achieved. As no outer normal stress was applied, it was assumed that the normal stress, σ_n, was zero – this is also an approximation as there can be normal stress locally in the joint, while the overall equilibrium demands that the average normal stress is zero. By inserting these approximations in equation (2), an approximate value of the coefficient of friction, μ, was obtained. After that, μ was adjusted to get the FEA to correspond to the experiments. The calibrated value of μ was 3.7 for Hedared and 1.33 for Abetong case 1 and 2.1 for Abetong case 2, see Figure 36. In a first step an approximate value of the elastic stiffness D_{22} was determined by the elastic stiffness in the test results, from the shear stress divided by the shear deformation. The elastic stiffness D_{22} was then adjusted until the stiffness of the elastic part corresponded between the FEA and the experiments. The calibrated values of D_{22} were $4.0 \cdot 10^{10}$ N/m^3 for Hedared and $3.5 \cdot 10^{10}$ N/m^{3}Abetong.

When the wedge split tests and shear tests were calibrated with high accuracy, the values were used as input for the full-scale model FEA. Final calibrated inputs for the FEA for all different cases are listed in Table 9.

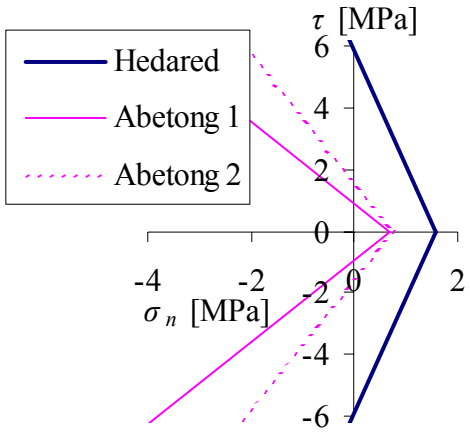

Figure 36 Friction model for all three cases

Table 9 Calibrated parameters of the joint model, input for FEA.

Parameter	Hedared	Abetong 1	Abetong 2
μ [-]	3.7	1.33	2.1
η [-]	0.5	0.5	0.5
D_{11} [N/m^3]	$3 \cdot 10^{11}$	$3 \cdot 10^{11}$	$3 \cdot 10^{11}$
D_{22} [N/m^3]	$4 \cdot 10^{10}$	$3.5 \cdot 10^{10}$	$3.5 \cdot 10^{10}$
f_{a1} [MPa]	1.58	0.69	0.75
κ_1 [mm]	0	0	0
f_{a2} [MPa]	0.599	0.109	0.109
κ_2 [mm]	0.033	0.05	0.05
f_{a3} [MPa]	0	0	0
κ_3 [mm]	0.11	0.17	0.17
G_F [N/m]	59	27	29

3.7 Results of analyses of shear tests

The load versus vertical joint slip from the FEA and the shear tests are presented in Figure 37. The vertical joint slip in the analyses was evaluated in a similar way as it

was measured in the tests, to ease the comparison. It was calculated as the difference in displacements in nodes that were situated where the measuring devices were placed in the tests, see Figure 37d. Figure 37a shows the result for Hedared. The FEA was without cracks, which leads to a linear response until the peak load, while horizontal cracking occurred in the tests. This explains the difference in the total joint slip for higher loads. For lower loads, both the force and the slip agree well between the FEA and the tests; in the analyses the same stiffness is found until collapse of the joint. As can be seen, the maximum load in the analyses corresponds well with the measured ones; this is as can be excepted as input for the cast joint was calibrated until agreement was found. Furthermore, the behaviour after maximum load is very brittle in the analyses; in the tests it could most often not be followed as it was too brittle.

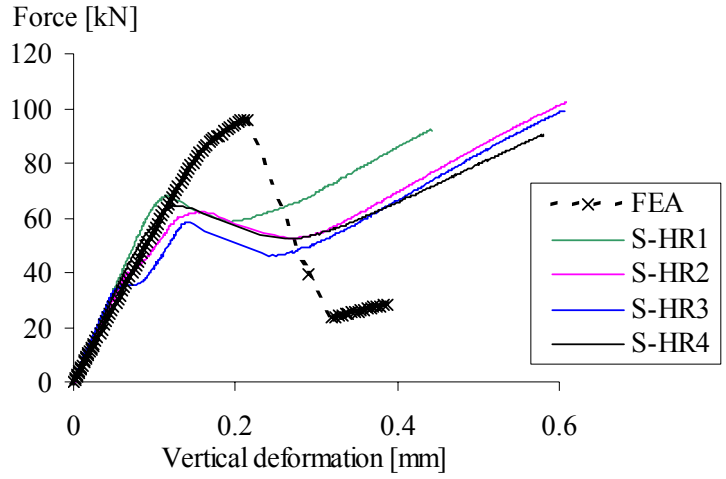

(a)

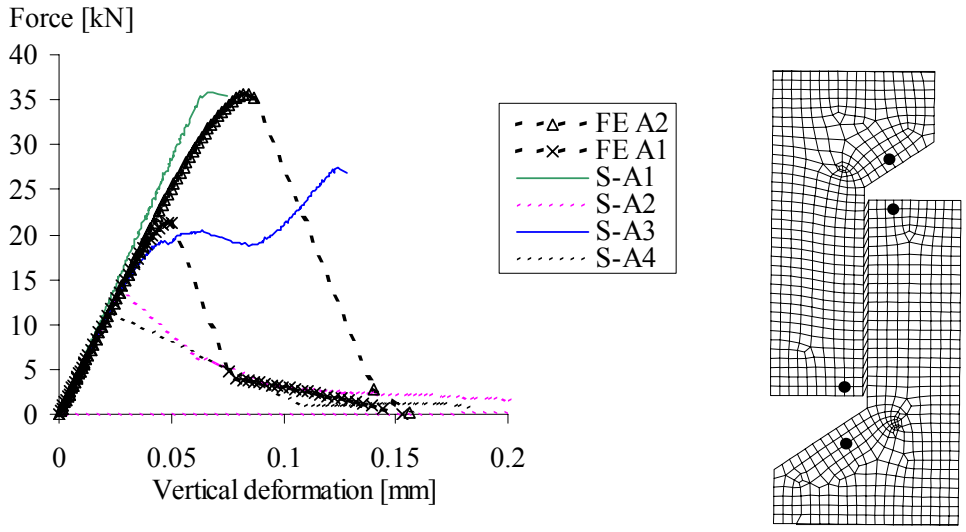

(b) (c)

Figure 37 *Comparison of load versus vertical deformation over the cast joint in shear tests and analyses, a) Hedared, b) Abetong case 1 and 2. c) The vertical deformation over the joint was calculated as the average of the differences in vertical displacements in the marked nodes (deformed mesh shown).*

The normal deformation over the cast joint obtained in the FEA and the experiments is compared in Figure 38. Slightly larger horizontal deformations were measured in the tests than was obtained in the analyses. However, the trend with increasing horizontal deformation just before and especially at maximum load is similar.

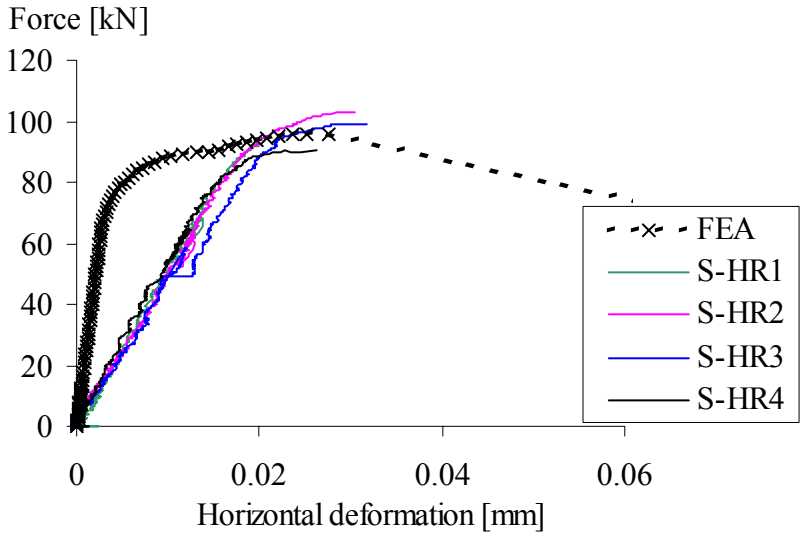

(a)

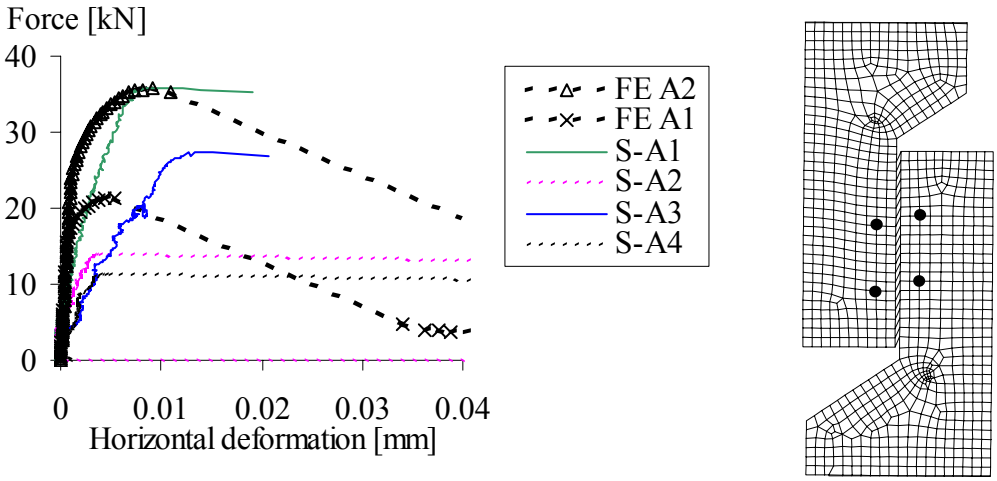

(b) (c)

Figure 38 *Comparison of load versus horizontal deformation over the cast joint in shear tests and analyses, a) Hedared, b) Abetong case 1 and 2. c) The horizontal deformation over the joint was calculated as the average of the differences in horizontal displacements in the marked nodes (deformed mesh shown).*

3.8 Results of analyses of wedge split tests

The load versus CMOD from the WST and the FEA of them are compared Figure 39. As can be seen, the results correspond well, which indicates that the parameters of the

joint are properly calibrated. The analyses converged until the CMOD was 0.2 mm for Hedared and 0.15 mm for Abetong; as can be seen in Figure 39 the solutions thereafter were unstable.

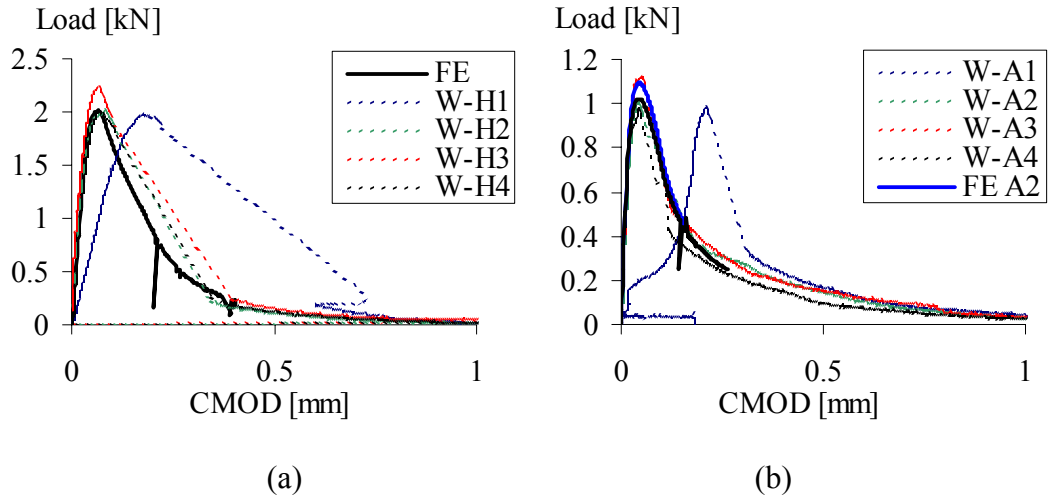

Figure 39 *Load versus CMOD for wedge split tests and finite element analyses of them. a) Hedared, b) Abetong case 1 and 2.*

3.9 Results of analyses of full-scale tests

The FEA of full-scale and test results were compared. As mentioned before Abetong was divided into two cases; Abetong case1 with joint capacity based on average test values and Abetong case 2 with joint capacity based on the highest test values in the calibration. Hedared had one case and the capacity of the joint was based on average test values in the calibration. In all analyses, a main crack appeared in the *in situ* cast concrete above the joint. Convergence problem occurred in the FEA for all three cases instantly after the first crack, but the problem was only for a few steps in FEA. In the analysis of Hedared, failure was determined by rupture of the reinforcement, as in the tests. However, in the analysis of Abetong (both case 1 and case 2), the cast joint fractured. In the following, each analysis is described more in detail.

3.9.1 Hedared

Load versus mid-span deflection from the tests and analysis of Hedared's test specimens is shown in Figure 40. As can be seen, there is a good agreement for the first part of the curves, with cracking at a load of about 11 kN and yielding at a load of about 19 kN. Crack patterns are compared in Figure 41; as can be seen there was mainly one crack in the *in situ* cast concrete above the joint in both the tests and in the analysis.

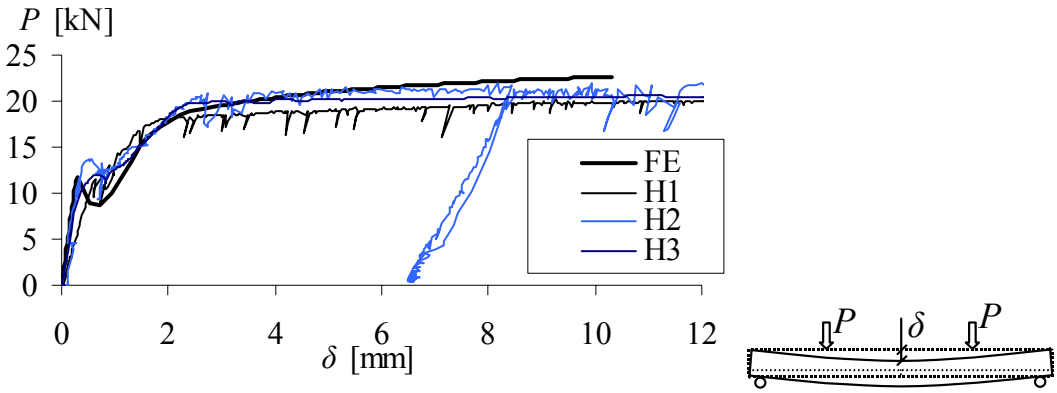

Figure 40 *Load versus mid-span deflection, in FEA and tests of Hedared's test specimens.*

Figure 41 describes the crack pattern just before collapse of the structure. One main crack, in the *in situ* cast concrete above the joint in the midspan, was formed. Smaller cracks were also formed at the first cross-bars in the reinforcement mesh over the joint; these were however very small.

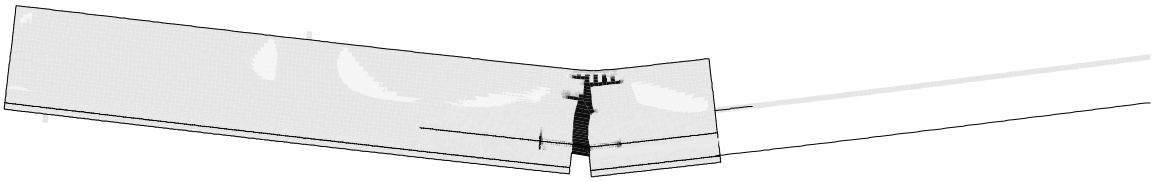

Figure 41 *Crack pattern (dark areas are cracked) and deformed structure before collapse. Contour plot of principal strain ε_1, with a scale ranging from 0 (white) to $1 \cdot 10^{-3}$ (black), from the analysis of tests specimens from Hedared.*

In Figure 42, the deformation in the cast joint is plotted versus the mid span deflection. As can be seen, both the horizontal slip and the vertical opening were rather small, and, most of all, it did not increase for large mid span deflections. Thus, the cast joint did not limit the capacity; the failure mode was rupture of the reinforcement. The strain in the reinforcement in the crack is shown in Figure 43; as can be seen maximum reached value is about 7.0%. This can be compared with the input, see Figure 33, where maximum stress is obtained at a strain of 7.7% and very brittle behaviour is assumed for strains larger than 8.6%. Thus, it can be concluded that failure in this case was determined by rupture of the reinforcement.

The reason for the large difference in the mid span deflection when rupture of the reinforcement bar occurs in the tests and in the analysis depends on the assumed bond-slip relation. In reality, the bond stress will drop when the reinforcement starts yielding. This was not included in these analyses; therefore, they are not capable of predicting a correct mid span deflection when rupture of the reinforcement occurs.

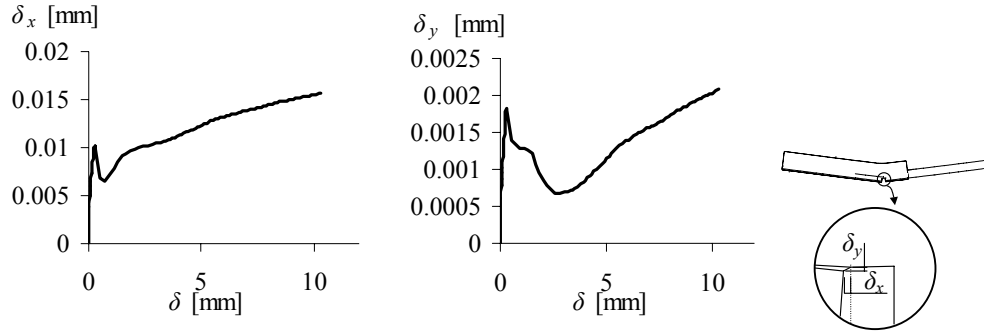

Figure 42 *Load versus deformation in the cast joint in the analysis of tests specimens from Hedared.*

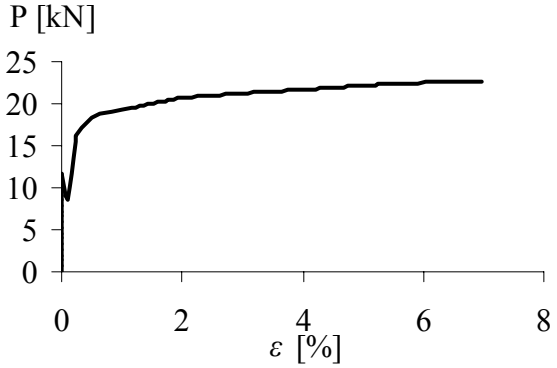

Figure 43 *Load versus strain in the reinforcement at the crack. From the analysis of test specimens from Hedared.*

3.9.2 Abetong

Load versus mid-span deflection from the tests and analyses of Abetong's test specimens is shown in Figure 44. As can be seen, there is a good agreement for the first part of the curves, with cracking at a load of about 11 kN and yielding at a load of about 19 kN. However, both of the analyses stop at a mid span deflection which is a lot smaller than was obtained in the tests; analysis Abetong case 1 stops at mid span deflection 3.8 mm and analysis Abetong case 2 at 7.9 mm.

Crack patterns in the analyses are shown in Figure 45; as can be seen there was one main crack in the *in situ* cast concrete above the joint in both of the analyses, similar as in the tests. However, there was also in both of the analyses of Abetong's test specimens one crack that appeared at the location of the first cross-bar in the reinforcement mesh, which appeared just before maximum load. Most likely, the appearance of this crack initiated opening of the joint, which was the failure mode in both these analyses. This can be seen in Figure 46, where the deformation in the joint is plotted versus the mid span deformation. As can be seen, the opening of the joint increased just before the analysis could not be continued; this indicates that the joint was limiting. This is further confirmed in Figure 47, where the strain in the

reinforcement in the main crack is plotted versus the load. As can be seen, the strain is well below the level where fracture of the reinforcement occurs; thus the failure mode in the analyses was opening of the grouted joint.

This is opposite to what was found in the tests; where the final failure mode was rupture of the reinforcement. One reason for the difference might be the choice of tying the reinforcement to the concrete at the locations of the cross-bars of the reinforcement mesh. This might have caused too large restraints in the analyses compared to the experiments, and therefore the second crack was initiated too easily in the analyses. This is confirmed when the strain in the reinforcement in the analyses is compared to what was measured in the tests, see Figure 48. Only results from analysis Abetong case 1 are shown, however, the results were similar also in the analysis of Abetong case 2 and Hedared.

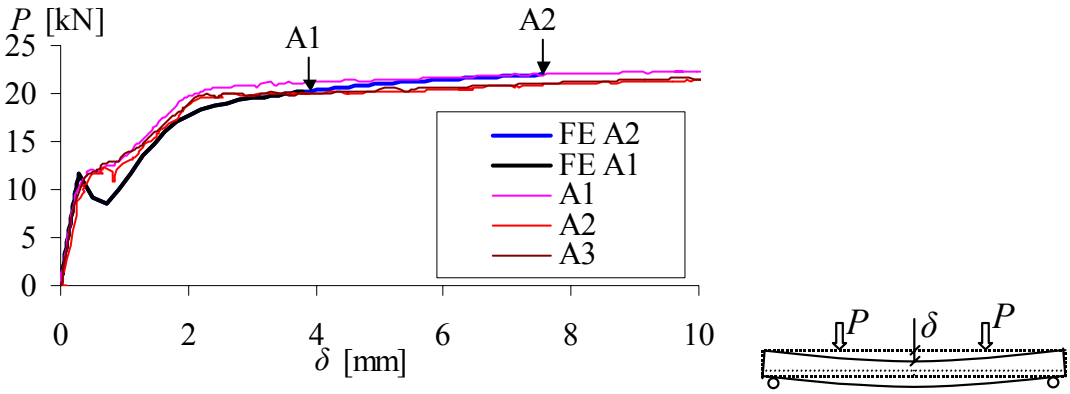

Figure 44 *Load P versus mid-span deflection, in FEA and tests of specimens from Abetong. Especially marked are the points were the FE analyses stopped.*

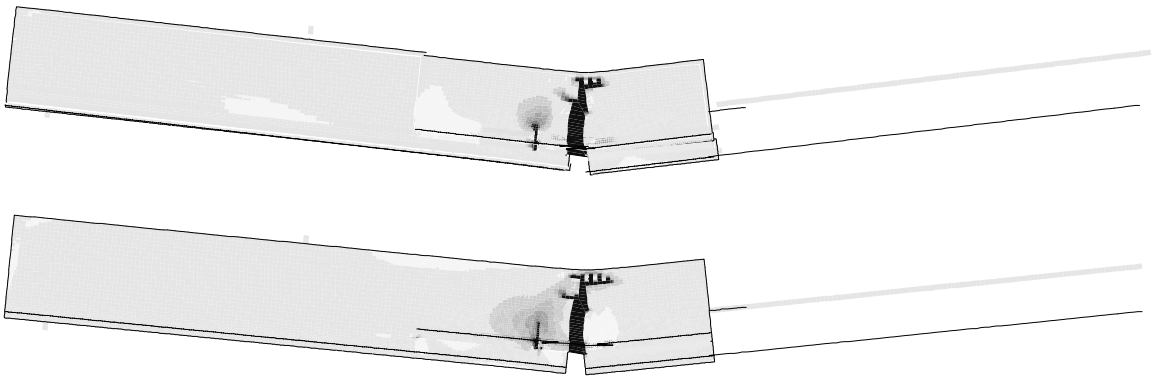

Figure 45 *Crack pattern and deformed mesh before collapse a) Abetong case 1, and b) Abetong case 2. Contour plot of principal strain ε_1, with a scale ranging from 0 (white) to $1 \cdot 10^{-3}$ (black).*

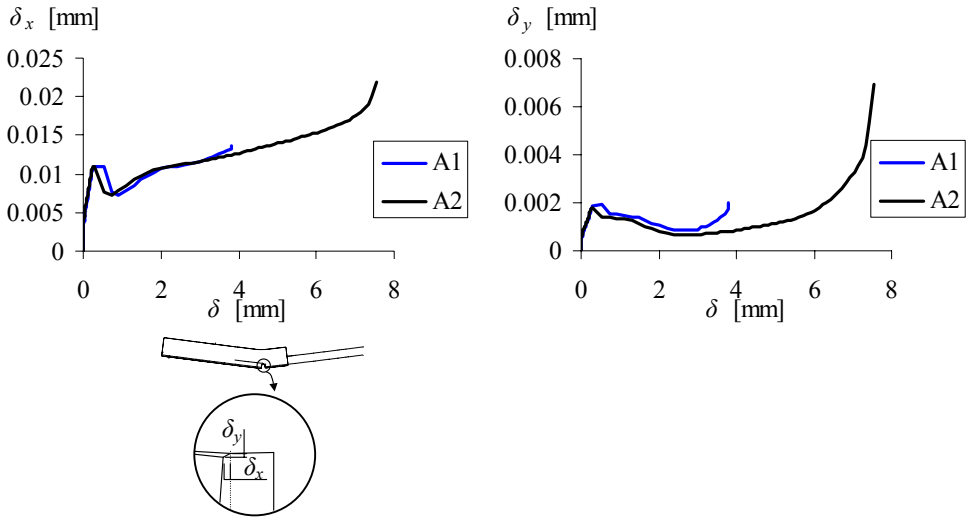

Figure 46 *Load versus deformation in the cast joint in the analysis of tests specimens from Abetong.*

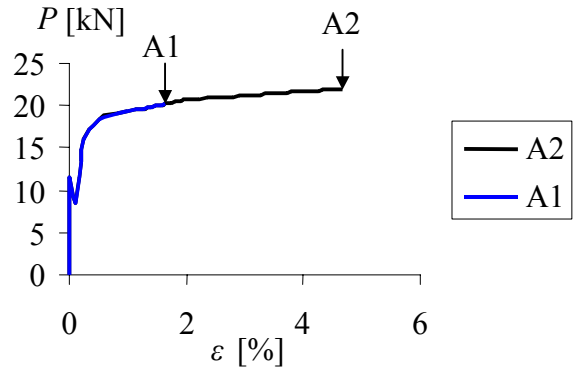

Figure 47 *Load versus strain in the reinforcement at the crack. From the analysis of test specimens from Abetong. Especially marked are the points were the FE analyses stopped.*

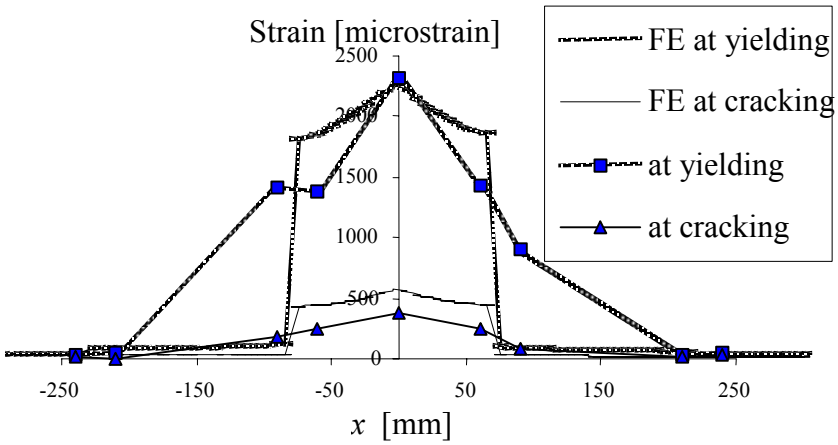

Figure 48 *Strain in the reinforcement at some load levels. From test specimen A1 and analysis Abetong case 1.*

When studying the measured strains along the reinforcement bar across the joint, it was clear that the cross-bars had provided very little restraints, as there was no distinct increase in strain at the location of the cross-bars. To better correspond to this situation, analysis Abetong case 1 was rerun without the tyings between the reinforcement and the concrete at the locations of the cross-bars. This analysis was denoted Abetong case 1b.

Load versus mid-span deflection from the tests and analysis Abetong case 1b is shown in Figure 49. As can be seen, the maximum obtained mid span deflection was a lot larger in this analysis than when the tyings were included; 12.2 mm compared to 3.8 mm. The failure mode in this analysis was rupture of the reinforcement with only one crack in the *in situ* cast concrete above the joint, similar as in the tests. This can be seen in Figures 50-52. In Figure 51, the deformation in the cast joint is plotted versus the mid span deflection. As can be seen, both the horizontal slip and the vertical opening were rather small, and, most of all, it did not increase for large mid span deflections. Thus, the cast joint did not limit the capacity. The strain in the reinforcement in the crack is shown in Figure 52; as can be seen maximum reached value is about 7.1%. This can be compared with the input, see Figure 33, where maximum stress is obtained at a strain of 7.7%. Thus, it can be concluded that failure in this case was determined by rupture of the reinforcement. In Figure 53, the strain in the reinforcement in the analysis is compared to measured for two load levels. As can be seen, a rather good agreement is found when no tyings were assumed between the reinforcement and the concrete; a lot better than when the tyings were present, compare Figure 48.

Thus, it can be concluded that the analysis without tyings better represent the tested specimen than the analysis with tyings at the locations of the cross-bars in the reinforcement mesh. This conlusion is based on that the failure mode in the analysis without tyings correspond to the one obtained in the test, and that the strain along the reinforcement bar better correspond to measured values. Furthermore, it can be concluded that the restraint of the cross-bars have a negative influence on the behaviour. It is important to note that in the tested specimens, the reinforcement mesh was placed directly on the precast concrete, without any distances. It is therefore most likely that the cross-bars were not very well-confined, and therefore did not contribute

to any major restraints. If, however, the reinforcement mesh was turned upside down, with the reinforcement crossing the joint directly on the precast concrete, a situation with better confined cross-bars would be achieved. Following from the analysis results here, this would not be beneficial.

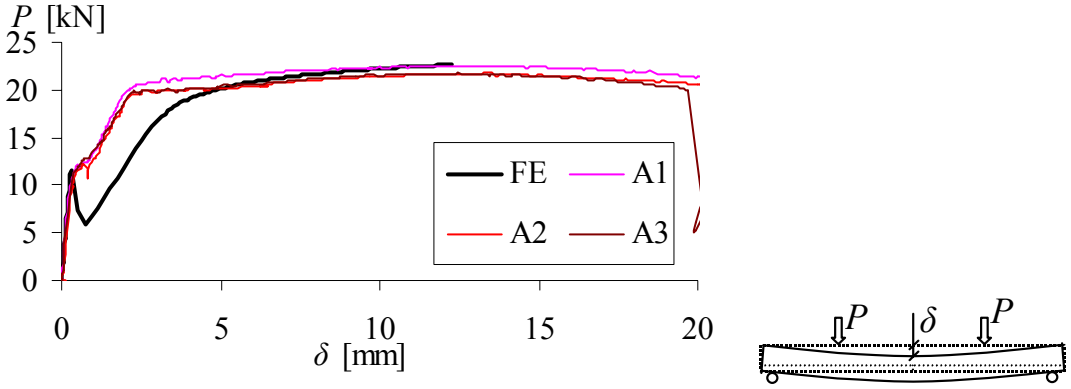

Figure 49 *Load P versus mid-span deflection, in FEA Abetong case 1b and tests of specimens from Abetong.*

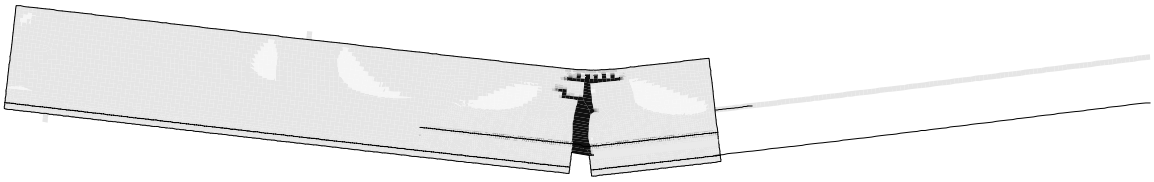

Figure 50 *Crack pattern and deformed mesh before collapse, Abetong case 1b. Contour plot of principal strain ε_1, with a scale ranging from 0 (white) to $1 \cdot 10^{-3}$ (black).*

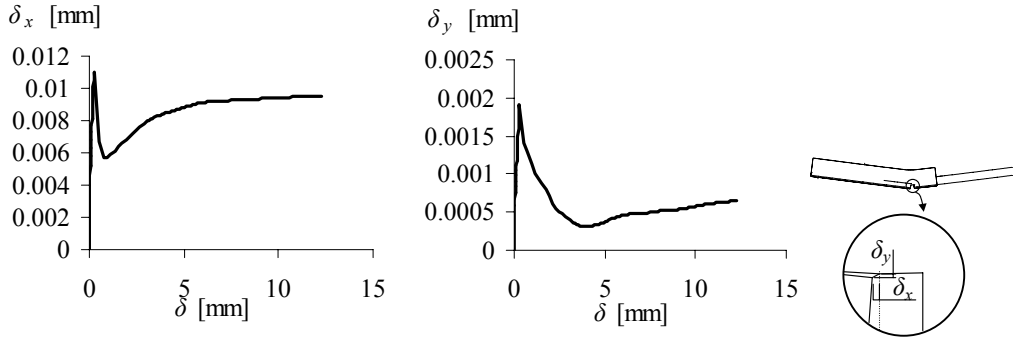

Figure 51 *Deformation in the cast joint versus mid span deflection in the analysis Abetong case 1b.*

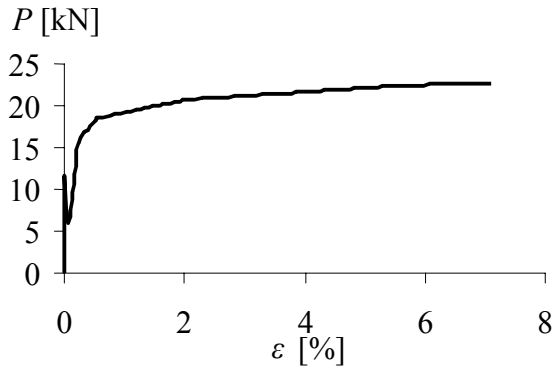

Figure 52 *Load versus strain in the reinforcement at the crack. From the analysis Abetong case 1b.*

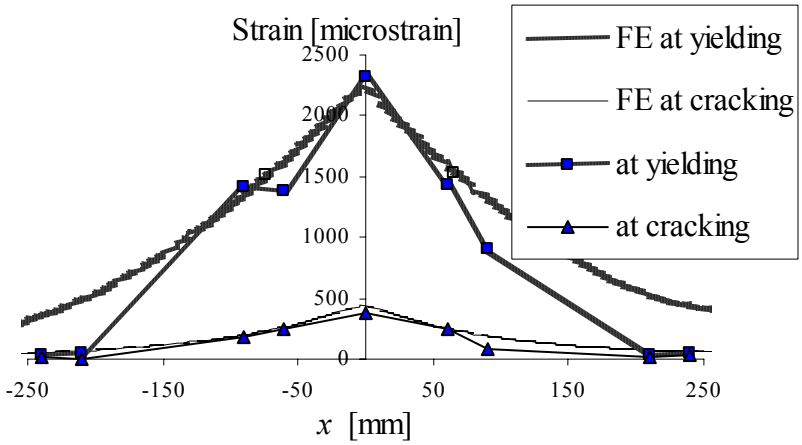

Figure 53 *Strain in the reinforcement at some load levels. From test specimen A1 and analysis Abetong case 1b.*

3.10 Effect of shear stresses in two directions

The tests and finite element analyses carried out were in 2D, with load-carrying only in one direction. However, in real applications, the slab will be load-carrying in two directions. The load-carrying in the main direction will also create shear stresses in the cast joint, which will be added to the ones investigated in this work. These shear stresses will be largest toward the supports. These shear stresses can be calculated as

$$\tau_y = V \cdot \frac{h(H-h)}{b \cdot H^3} 6 \qquad (4)$$

when the slab is uncracked, and

$$\tau_y = \frac{V}{b \cdot z} \approx \frac{V}{b \cdot 0{,}9d} \qquad (5)$$

when the slab is cracked. In these expressions, τ_y is the shear stress in the main load-carrying direction, V is the shear force, h is the height of the prefabricated part of the slab, H is the total height of the slab, b is the width of the slab, and d is the distance from the upper edge to the reinforcement. In section 3.12, a slab with a span of 7.0 m in the load-carrying direction was analysed. Maximum applied distributed load was then below 17 kN/m^2. For this slab, the maximum shear force can then be calculated as

$$V = q \cdot \frac{l}{2} = 17 \cdot \frac{7}{2} = 59.5 \text{ kN/m}$$

if only loading in the main direction is considered. This value is high, as the applied load would be lower if load-carrying was only possible in the main direction. The shear force will cause a shear stress in the cast joint of

$$\tau_y = V \cdot \frac{h(H-h)}{b \cdot H^3} \cdot 6 = 59.5 \cdot 10^3 \cdot \frac{0.05(0.25-0.05)}{1 \cdot 0.25^3} \cdot 6 = 0.228 \text{ MPa}$$

or

$$\tau_y \approx \frac{V}{b \cdot 0.9d} = \frac{59.5 \cdot 10^3}{1 \cdot 0.9 \cdot 0.225} = 0.294 \text{ MPa}$$

depending on if the slab is considered to be cracked. In the following, a simplified way to take this shear stress into account in the analyses is outlined. A basic assumption is that the cast joint has the same properties for shear loading in both directions. This assumption is indeed questionable for the surface with single grooves, while it is more likely for the brushed surface. However, here the assumption is only used for the brushed surface. Furthermore, it is assumed that the earlier calibrated model of the cast joint is valid for the resulting shear stress:

$$\tau = \sqrt{\tau_x^2 + \tau_y^2} \,. \tag{6}$$

By inserting this expression in equation (2), the shear stress in x-direction is limited by

$$\sqrt{\tau_x^2 + \tau_y^2} + \mu \cdot (\sigma_n - f_a) = 0 \,. \tag{7}$$

By using an upper value of τ_y, the effect of the yield lines on shear stresses in the perpendicular direction can be investigated. Thus, the slab was assumed to be cracked, corresponding to τ_y = 0.294 MPa. The effect this has on the yield line in the τ_x-σ_n plane for the calibration of Hedared's test specimens is shown in Figure 54. As can be seen, the effect is very small, and can in a simplified way be taken into account by reducing the adhesive strength; in this case from 1.58 MPa to 1.50 MPa. This was done in analyses in next section.

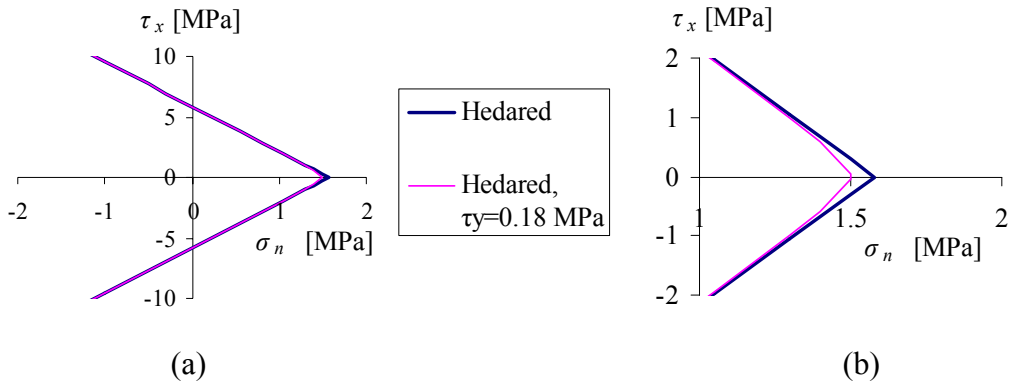

Figure 54 *Effect of a shear stress in the y-direction on the yield lines in the τ_x-σ_n plane, a) overall, and b) part at the corner enlarged.*

3.11 Parameter study in analyses of full-scale tests

It was clear that the grouted joint had capacity enough not to be limiting in the full-scale tests. This result could also be found in the analyses: for Abetong's test specimens the joint was not limiting when the restraints from the cross-bars in the reinforcement mesh was not included, while for Hedared's test specimens the joint was not limiting even when the restraint was included. One very important question is how large safety there is with the tested design of the joint. For Abetong's test specimens, the analyses in the previous chapter already indicate this: if the cross-bars in the reinforcement mesh were more confined than in the present test, the joint would most likely be limiting. Therefore, it can not be recommended to use the studied detailing for load-carrying purposes with prefabricated elements with this type of surface.

Hedared's test specimens, on the other hand, managed to reach rupture of the reinforcement in the analyses even when full restraint was assumed between the cross-bars and the concrete. The question is therefore how sensitive the detailing is. To investigate this, some variations were examined. The parameters describing the cast joint obviously have a very strong influence on the behaviour of the structure. These parameters will be influenced by the conditions when the cover concrete is cast *in situ*. The conditions on the construction place can be difficult to control: how can it for example be made sure that there is not dust, snow, or oil from formworks at the surface of the prefabricated concrete when the *in situ* concrete is cast? It was judged that this would mainly influence the adhesive strength. In the previous section it was shown that shear stresses in the other direction in a simplified way can be taken into account by decreasing the adhesive strength. Thus, there was a need to check through analyses how large effect on the results varying values of the adhesive strength will have. The coefficient of friction and also the other parameters of the joint are mainly dependant on the roughness of the surface. As this is created in factory, it is easier to control. These parameters were therefore not varied.

Thus, two more analyses were carried out:

- With half the adhesive strength as found in the calibration of the grouted joint.

- With zero adhesion in the grouted joint.

Other values in these two analyses were chosen as in the analysis of Hedared's test specimens.

The results from analyses with half adhesive strength are shown in Figures 55-58. As can be seen, the limiting failure mode was rupture of the reinforcement. Only one main crack appeared, even if smaller cracks are visible at the position of the cross-bars of the reinforcement mesh. However, opening of the joint is most likely rather close in this case; it can be seen in Figure 57 the opening increased just before the analysis could not be continued.

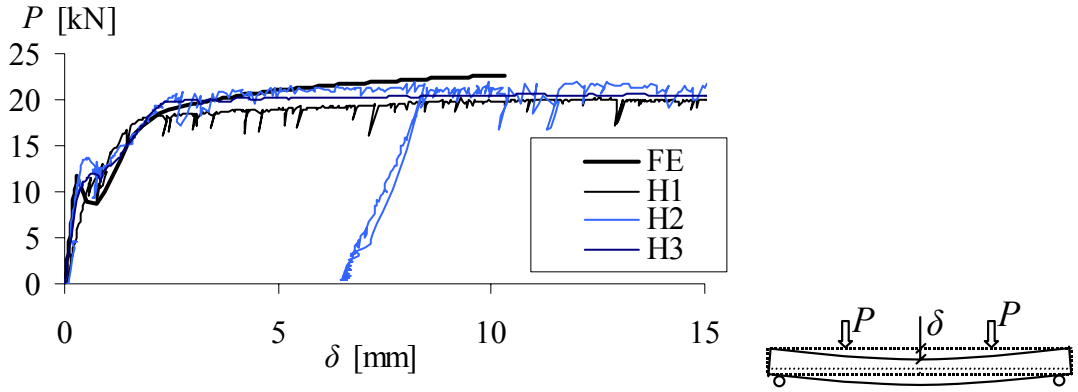

Figure 55 *Load P versus mid-span deflection, in FEA Hedared with half adhesive strength and tests of specimens from Hedared.*

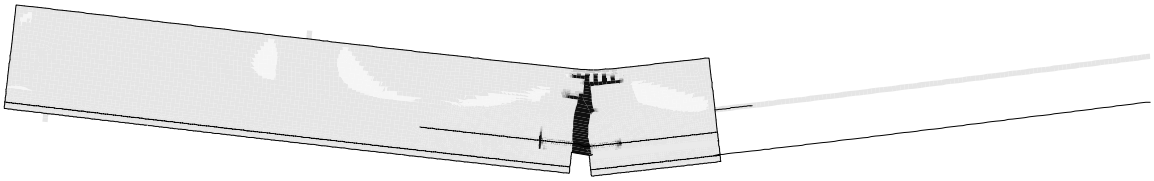

Figure 56 *Crack pattern and deformed mesh before collapse. From the analysis Hedared with half adhesive strength.*

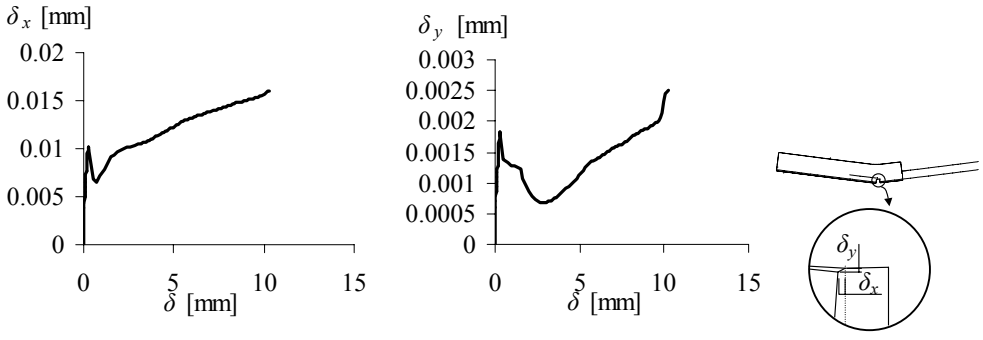

Figure 57 *Deformation in the cast joint versus mid span deflection in the analysis Hedared with half adhesive strength. Contour plot of principal strain ε_1, with a scale ranging from 0 (white) to $1 \cdot 10^{-3}$ (black).*

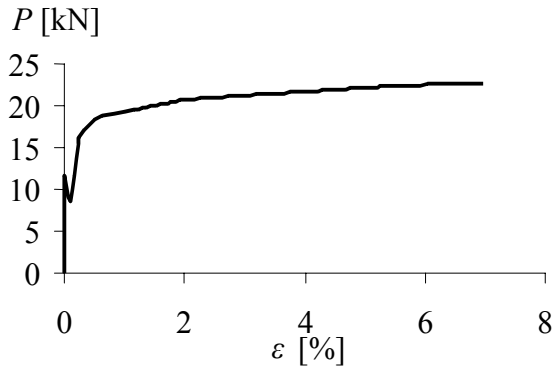

Figure 58 *Load versus strain in the reinforcement at the crack. From the analysis Hedared with half adhesive strength.*

The results from analyses with zero adhesion are shown in Figures 59-62. As can be seen, the limiting failure mode was opening of the joint before yielding of the reinforcement could be reached. At maximum load, a bending crack at the lattice girder truss appears. Then, the cast joint opened up, and thus limited the maximum load.

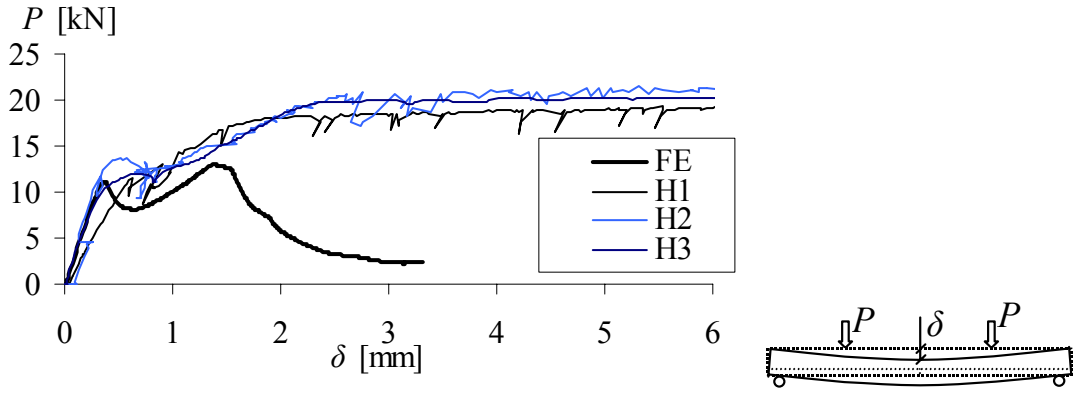

Figure 59 *Load P versus mid-span deflection, in FEA Hedared without adhesion and tests of specimens from Hedared.*

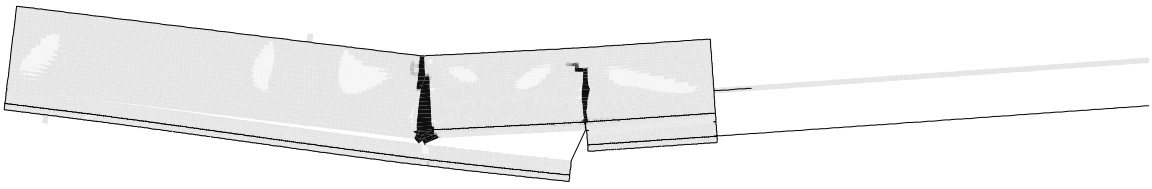

Figure 60 *Crack pattern and deformed mesh before collapse, Hedared without adhesion. Contour plot of principal strain ε_1, with a scale ranging from 0 (white) to $1 \cdot 10^{-3}$ (black). Note that the opening of the grouted joint is clearly visible, though it is not marked black.*

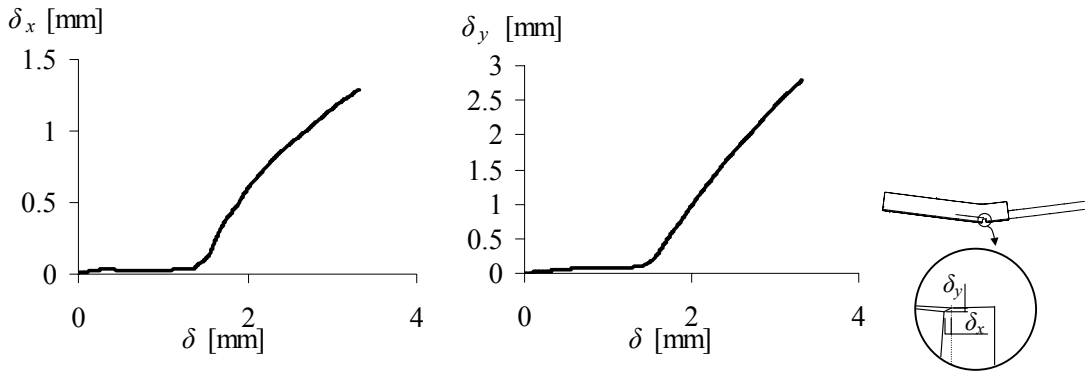

Figure 61 *Deformation in the cast joint versus mid span deflection in the analysis Hedared without adhesion.*

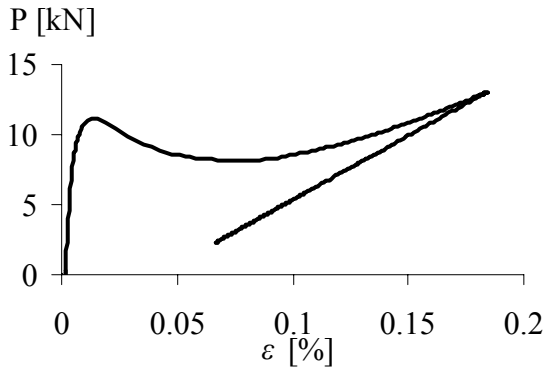

Figure 62 *Load versus strain in the reinforcement at the crack. From the analysis Hedared without adhesion.*

The results from all analyses of full-scale tests are summarised in Figure 63.

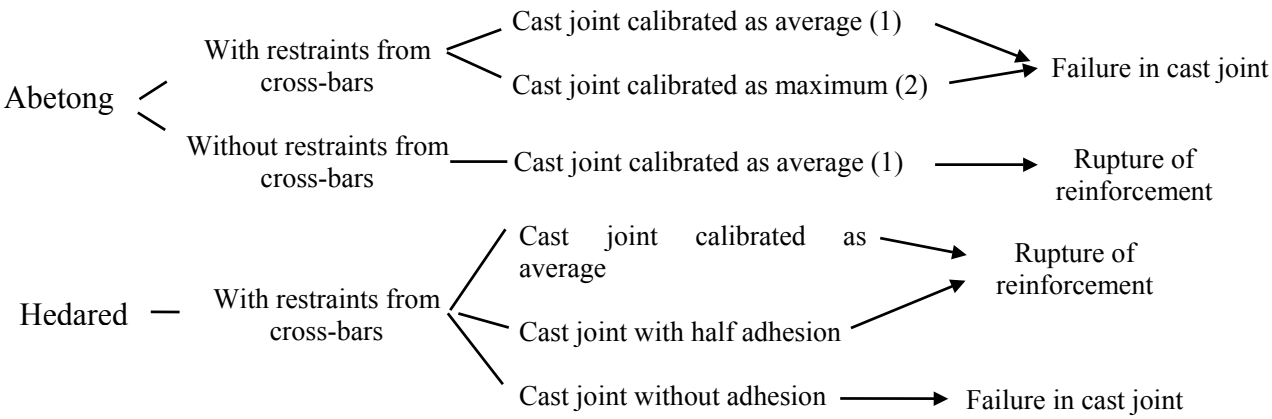

Figure 63 *Results from all analyses of full-scale tests summarised.*

3.12 Analyses of a slab

A slab was analysed to investigate the effect of the behaviour of the joint on the whole structure. The slab was 7 m * 7.2 m, consisting of three prefabricated elements and supported along all its four edges as shown in Figure 64a. It was loaded with an equally distributed load. The dimensions were chosen to be representative for the investigated lattice girder truss. The total height of the slab was 250 mm, and the reinforcement was Ø8 s150 NPs 500 in both directions. The distance *d* from the upper edge to the centre of the reinforcement was assumed to be 225 mm, the same for reinforcement in both directions. The properties of the joints were varied.

The symmetry was used so that only one fourth of the slab was modelled. Shell elements were used, see Figure 64b. Eleven integration points were used over the height, to be able to model the cracking of the slab. The joints between the prefabricated elements were modelled by non-linear rotation springs.

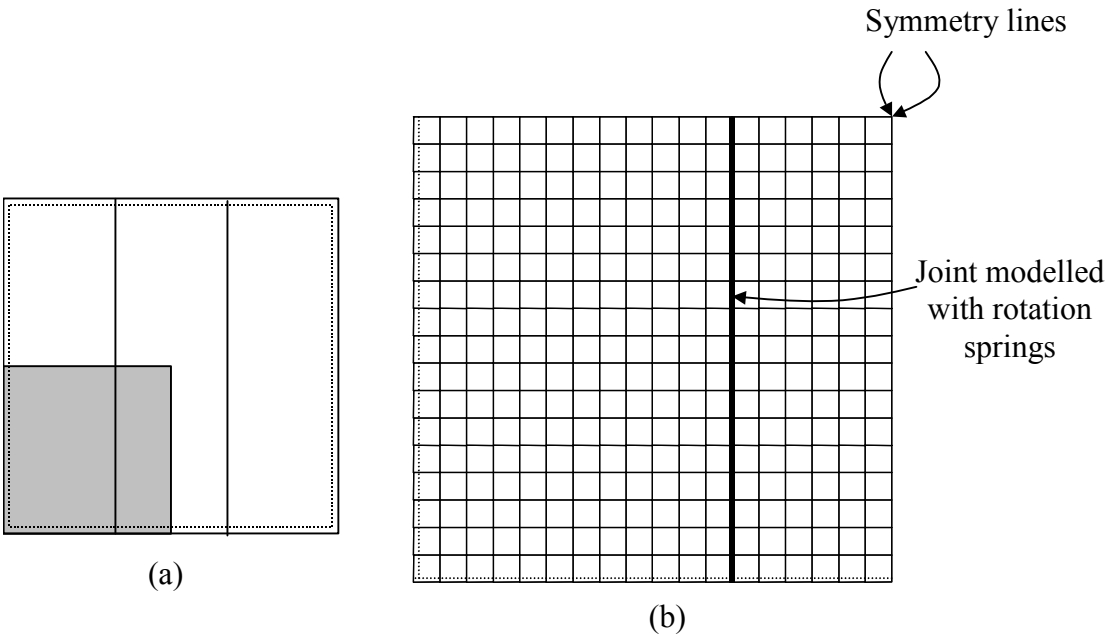

Figure 64 (a) Modelled slab, grey marked part modelled (b) with shell elements.

Two various set of input data for the concrete were used. In the first one, the concrete was assigned normal values of all parameters, see Table 10. In the second set of input data, the tensile strength was reduced to only one tenth of more realistic values. This was done to simulate that cracking of the slab had occurred at an earlier stage; either due to load or due to for example shrinkage and restraints. The reinforcement was modelled as ideal plastic, with Young's modulus 200 GPa and a yield strength of 500 MPa.

Table 10 Material data of the concrete used in the analyses of the slabs.

Concrete	f_{cc} [MPa]	E_c [GPa]	f_{ct} [MPa]	G_F [N/m]
Normal	36.5	33.2	2.80	74.3
Reduced	36.5	33.2	0.28	20.0

The properties of the joint were varied. In the analysis with the "normal" values of the concrete properties, the joint was given properties corresponding to the ones measured in the full-scale tests. In the other analyses, the joint was assumed to be cracked from the beginning, and the rotation capacity of the joint was varied. The various input curves are shown in Figure 65; they were denoted depending on their rotation capacity. It can be noted that the rotation is related to the deformations in the full-scale tests carried out within this work approximately as:

$$\varphi = \frac{\delta}{l} \cdot 4 , \tag{8}$$

where l is the span of the tested specimen, 2.5 m and δ is the mid span deflection of the tested specimen.

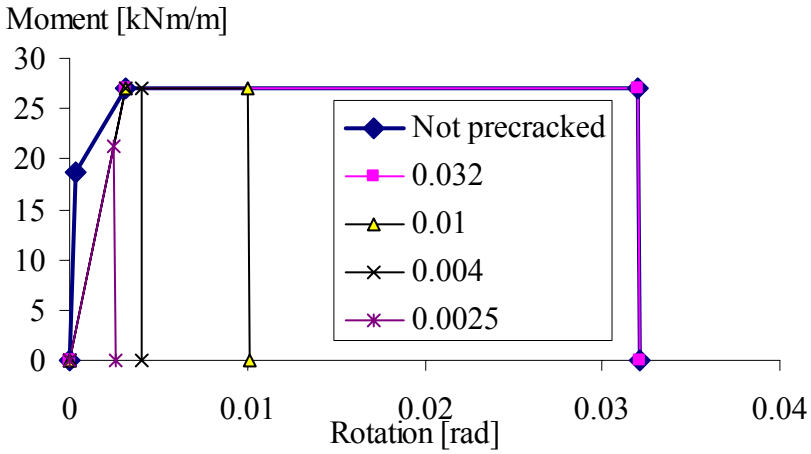

Figure 65 Various input chosen for the lattice girder joint in different analyses; bending moment versus rotation.

The load versus mid span deflection resulting from the analyses of the slabs are shown in Figure 66. It should be noted that in most of the analyses, the solution did not converge for high loads. Therefore, the absolute values of the maximum obtained loads should not be trusted. However, the errors were rather small; therefore the relation between the maximum load in the different analyses can be trusted. As can be seen, the maximum load increased with increasing rotation capacity. For the lowest rotation capacity, also the bending moment capacity was decreased (see Figure 65), to 21.2 kNm/m compared to 27.1 kNm/m in the other analyses. Naturally, this affected

the capacity of the slab, but note that the capacity of the slab was also affected when only the rotation capacity was changed, not the bending moment capacity. This depends on that a certain rotation capacity is needed to enable the full bending moment capacity to be mobilised in all needed parts of the slab. In Figure 67, the maximum load is plotted versus the rotation capacity. As can be seen, the maximum load increased with the rotation capacity. In Figure 66, it can also be seen that brittle failure of a joint leads to brittle failure of the slab. Therefore, it is recommended that the rotation capacity is not limited by the cast joint, but rather by rupture of the reinforcement bar.

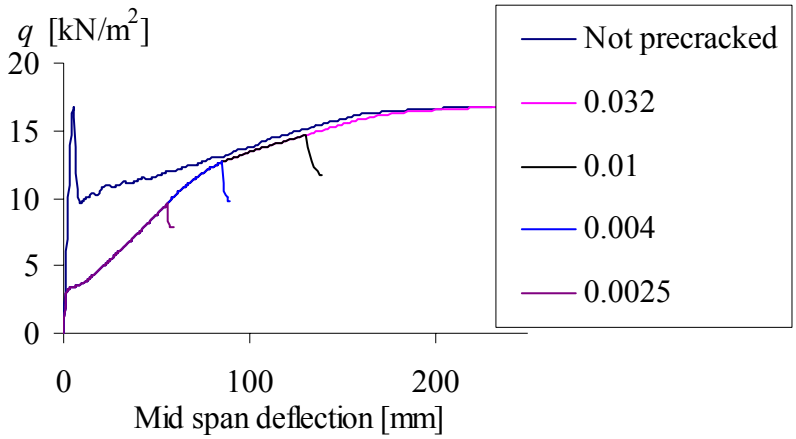

Figure 66 Load versus mid span deflection in analyses of slabs.

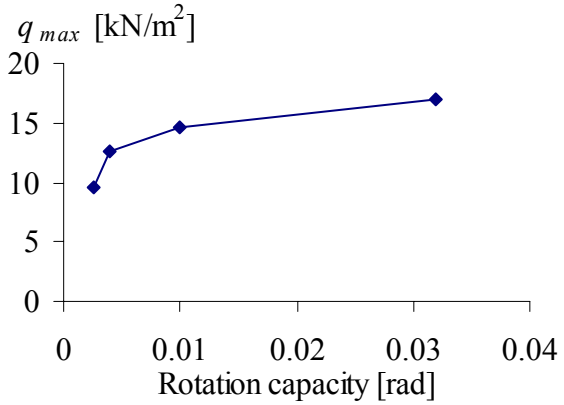

Figure 67 Maximum load versus rotation capacity in analyses of slabs.

In the analysis with the slab not precracked, a high first peak was obtained. At this high peak, the crack pattern developed; the crack pattern at two various steps are shown in Figure 68. For higher loads, the cracked region grows wider and wider. These results are similar also in the other analyses.

In Figure 69, the stresses in the reinforcement at maximum load are compare from two analyses. As can be seen, yielding is reached in large parts when the joint has a high rotation capacity. This is not the case when the rotation capacity is very limited.

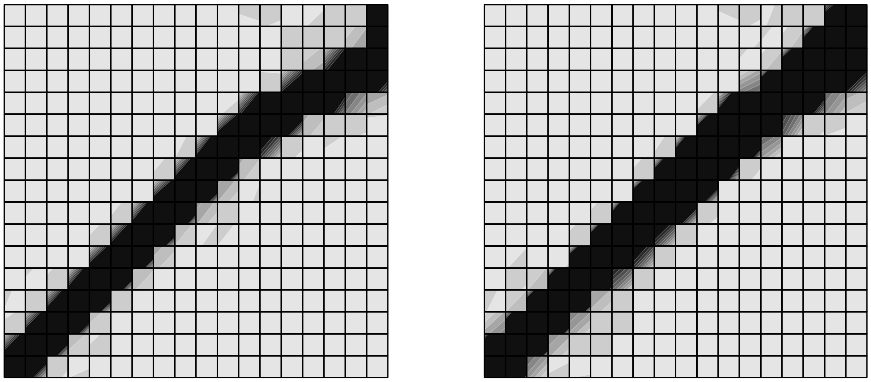

(a) (b)

Figure 68 *Crack pattern (dark areas indicate cracks) (a) just after the first peak, load q = 9.84 kN/m2, and (b) after further load increase, q = 10.40 kN/m2.*

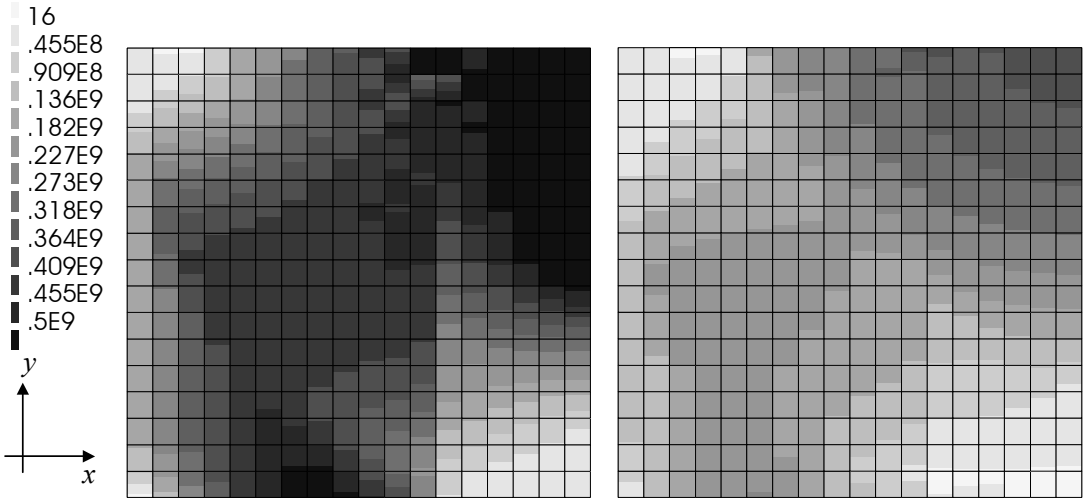

(a) *(b)*

Figure 69 *Contour plots of the stress in the reinforcement in the x-direction, in Pa. a) At maximum load in the analysis with rotation capacity 0.032 in the joint, and b) At maximum load in the analysis with rotation capacity 0.0025 in the joint.*

4 Conclusions

4.1 General conclusions

In the present study, the possibility to enable load-carrying in two directions in lattice girder slab systems by complementing with lapped reinforcement across the joints at the construction site was studied. The study was limited to a detailing without any reinforcement crossing the horizontal cast joint between the prefabricated and the *in situ* cast concrete. Two different surface treatments of the precast elements were studied: one was brushed and the other had single grooves. In the studied detailing of the joint, a reinforcement mesh was placed in the *in situ* concrete across the joint, directly on the surface of the precast elements.

Two types of detail tests of the cast joint were carried out: one type where the cast joint was loaded in shear and one in tension. Furthermore, the detailing of the joint between two precast concrete panels was tested in bending in full-scale tests. The detail tests were used to calibrate a model of the cast joint, which was then used in non-linear finite element analyses of the full-scale tests. The test specimens with surfaces with single grooves showed a large scatter in the detail tests loaded in shear; in all other tests the scatter was relatively low. Furthermore, the capacity of the cast joint was markedly higher for the brushed surface than for the surface with single grooves: maximum shear stress was around 4 MPa compared to 1 MPa, and the adhesive strength was around 1.6 MPa compared to 0.7 MPa.

In the full-scale tests, the cast joints were strong enough to carry the applied load. In all full-scale tests the failure mode was rupture after considerable yielding of the reinforcement, and only one crack occurred; in the *in situ* cast concrete above the joint between the precast elements. However, the finite element analyses of the full-scale tests revealed that the detailing was sensitive for secondary cracking; when restraints from the cross-bars of the reinforcement mesh initiated bending cracks, the failure mode changed to fracture of the cast joint in the analyses. This happened in the analyses where the precast surface was modelled with single grooves. In the analysis where the surface was modelled as brushed, no secondary cracking occurred even when the restraints from the crossbars were included in the analyses. It is worth to note that in the full-scale tests, the cross-bars were placed directly on the surface of the precast concrete; accordingly they were most likely not so well encased and did not cause any larger restraints.

Analyses of whole slabs were carried out to investigate the demands of the deformation capacity of the lattice girder joint. As can be expected, they show that the load-carrying capacity of a slab depends on the rotation capacity of the joints. Brittle failure of a joint leads to brittle failure of the slab. Therefore, it is recommended that the rotation capacity of the lattice girder joint is not limited by the horizontal cast joint, but rather by rupture of the reinforcement bar.

One very important question is how large safety there is with the tested detailing of the joint. The analyses of the specimens with surfaces with single grooves indicate that if the cross-bars in the reinforcement mesh were more encased than in the present test, the joint would most likely be limiting. Furthermore, the shear tests of the cast joint where the prefabricated surface had single grooves showed a very large scatter.

Therefore, prefabricated elements with surfaces with single grooves can not be recommended for use in the studied detailing without complementing reinforcement across the cast joint.

The test specimens with brushed surface, on the other hand, managed to reach rupture of the reinforcement in the analyses even when full restraint was assumed between the cross-bars and the concrete, and also when the adhesive strength of the joint was decreased to half of its calibrated value. When the adhesive strength of the joint was assumed to be zero, the cast joint failed. A minor decrease of the adhesive strength is reasonable to use due to the presence of shear stresses in the main load-carrying direction. Approximate analyses indicated that this corresponds to a decrease of about 5 %, and the results are thus promising. However, various effects on the construction site will affect the adhesive strength, such as dust, snow, or oil from formworks at the surface of the prefabricated concrete when the *in situ* concrete is cast. It is very important that these factors are under control if the studied detailing is to be used in practice. Furthermore, long-term effects such as shrinkage and creep were not included in this study; this must be investigated.

4.2 Preliminary design instructions

From the results in this study, it is concluded that the studied detailing of load-carrying joints between lattice girder slabs without any reinforcement across the cast joint is very sensitive to the roughness of the surface of the prefabricated elements. There is a risk of brittle failures; thus it raises questions whether reinforcement across the cast joint is needed to guarantee the structural integrity of a structure. It is further concluded that not all surfaces of the prefabricated elements used in Sweden today can be used. Furthermore, long-term effects such as shrinkage and creep were not included in this study; this must be investigated.

Considering this, it can however still be possible to use the studied detailing for load-carrying purposes. Very important demands are then that:

- The conditions at the work site must be controlled. The workers at site must be aware of how important it is that the surface of the prefabricated concrete is clean and not filthy with for example dust, snow, or oil from formworks when the *in situ* concrete is cast.

- The production of the surface of the prefabricated elements must be controlled and checked on regular basis. Brushed surface is recommended. Demands on the surface must be clearly stated and checked by for example shear tests as done in this study. These demands must include both the shear capacity and the shear stiffness of the joint.

Other design aspects are that:

- It is recommended that the joints should, whenever possible, be located away from the critical sections.

- Due to that cracking will mainly appear only in the joints, it is recommended that the reinforcement to be used in the joint should have a high ductility (not cold drawn).

- It is recommended to place the reinforcement mesh with the cross-bars down towards the prefabricated concrete, as was done in this study.

4.3 Suggestions for future research

As already mentioned, long-term effects such as shrinkage and creep were not included in the present study. This needs to be investigated.

The studied detailing had no reinforcement across the horizontal cast joint. By use of reinforcement across the cast joint, the structure would become a lot more robust, and could be designed to avoid brittle failures. The use of reinforcement across the cast joint would drastically decrease the needs for control of both the production of the surface of the prefabricated elements and the conditions at the work site. Therefore, it is recommended that this alternative is investigated, and that detailing with reinforcement layouts that lead to rational work on site are worked out.

5 References

CEB (1993): *CEB-FIP Model Code 1990*, Bulletin d'Information 213/214, Lausanne, Switzerland, 1993.

Helgesson J. and Sylvén R. (2005): *Analyses and experiments of joints in lattice girder structures*. Master thesis, Department of Structural Engineering and Mechanics, Concrete Structures, Chalmers University of Technology, Göteborg, 2005.

Karihaloo B. (1995): *Fracture Mechanics and Structural Concrete.*, Longman, Sydney, Australia, 1995.

Linsbauer H. N. and Tschegg E. K. (1986): Fracture energy determination of concrete with cube shaped specimens. *Zement und Beton*, Vol. 31, pp. 38-40.

Lundgren K. (2003): *Analysis of a lap splice in a lattice girder system*. Report 03:3, Chalmers University of Technology, Department of Structural Engineering, Concrete Structures, Göteborg.

Nissen I., Daschner F. and Kupfer H. (1986): *Versuche zur notwendigen Schubbewehrung zwischen Betonfertigteilen und Ortbeton (Tests of the necessary shear reinforcement between precast concrete elements and in situ concrete. In German)*. Deutscher Ausschuss für Stahlbeton, Berlin.

Østergaard L. (2003): *Early-Age Fracture Mechanics and Cracking of Concrete - Experiments and Modelling*. Ph.D. Thesis, Department of Civil Engineering, Technical University of Denmark, 2003.

TNO (2002): *DIANA Finite Element Analysis, User's Manual release 8.1*, TNO Building and Construction Research, 2002.

Appendix A. Photographs of surfaces


H3

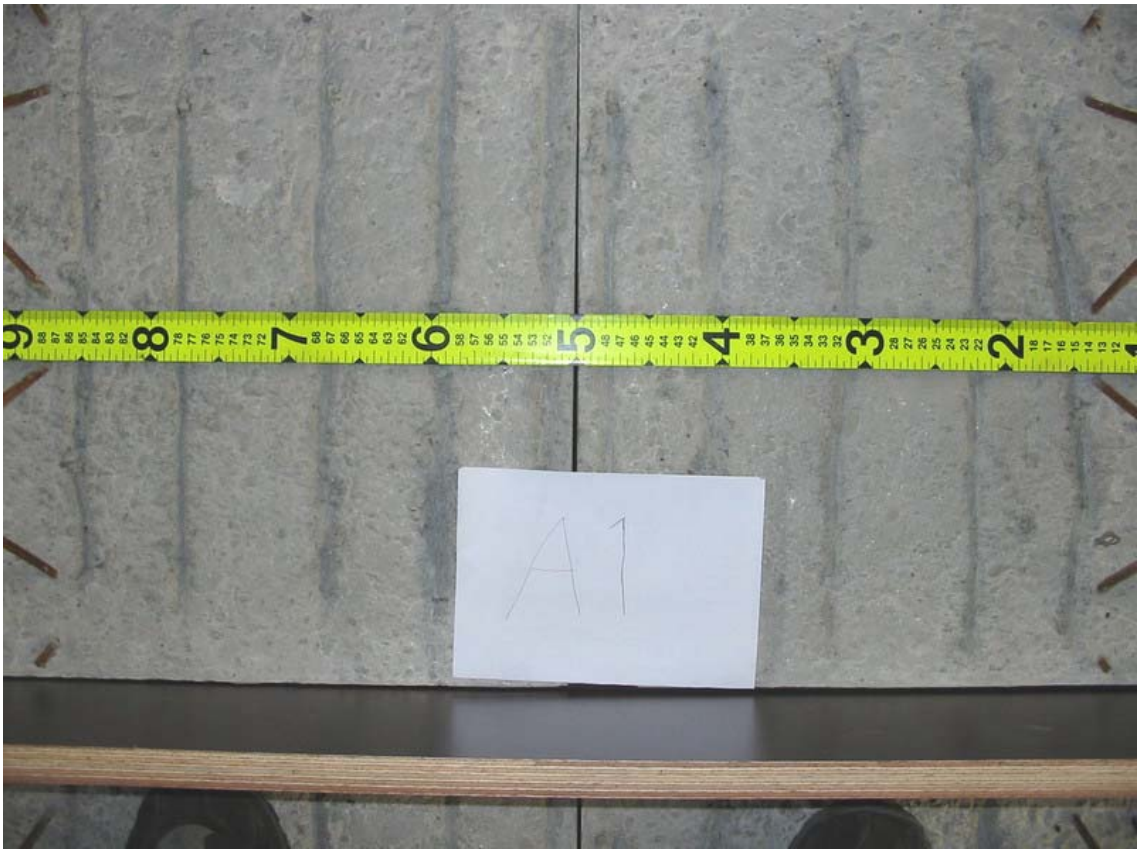
A1


A2

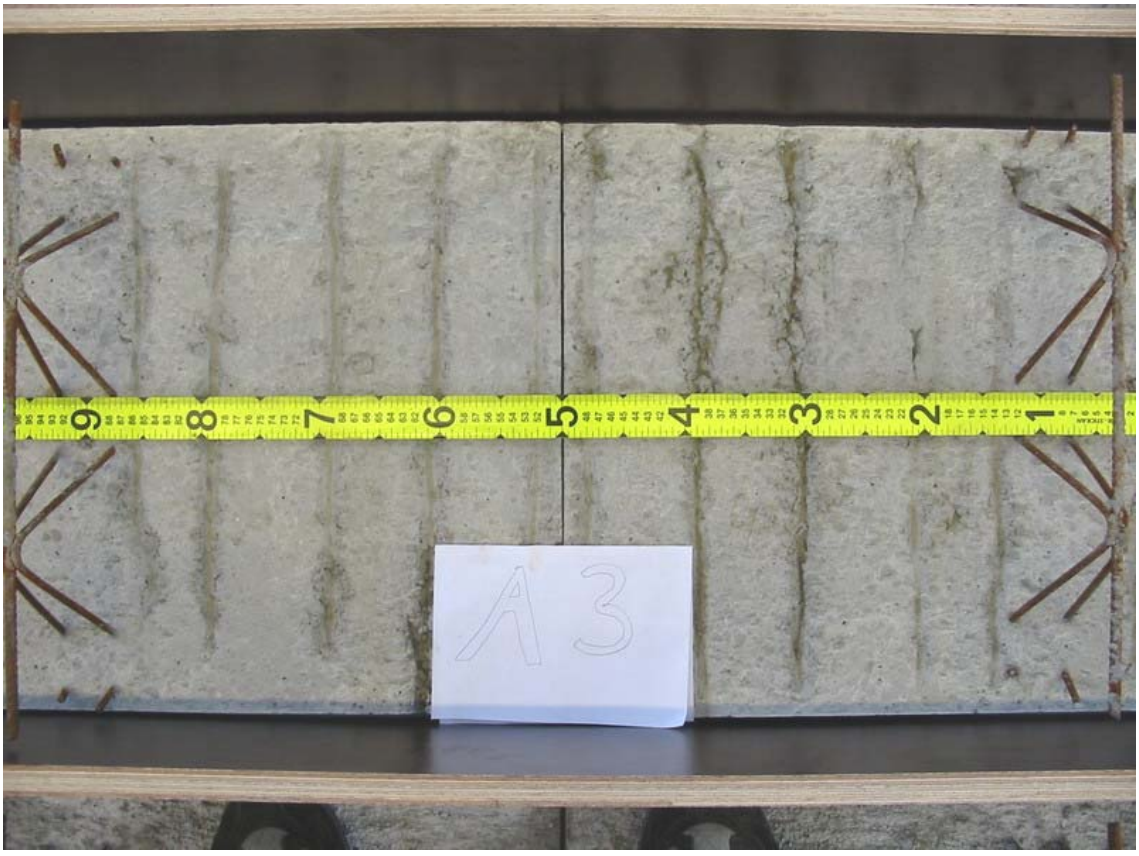
A3

Appendix B. Measurements in shear tests

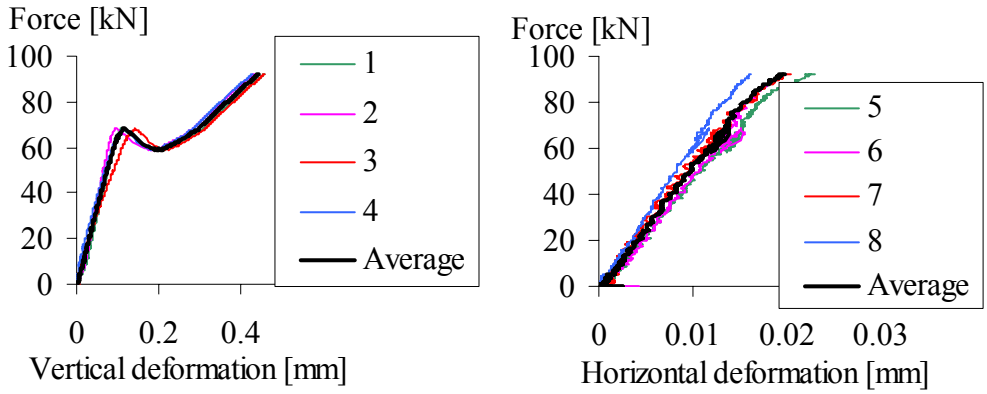

Figure B1 Measured displacements in test no. S-HR1.

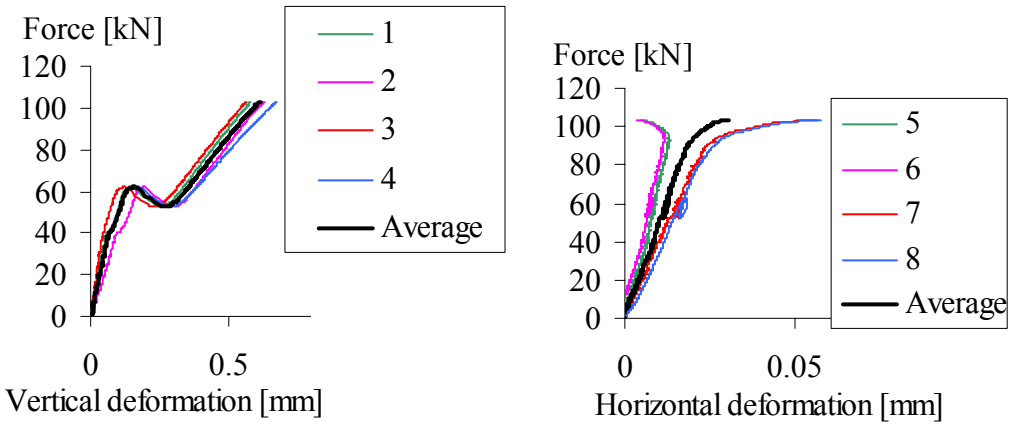

Figure B2 Measured displacements in test no. S-HR2.

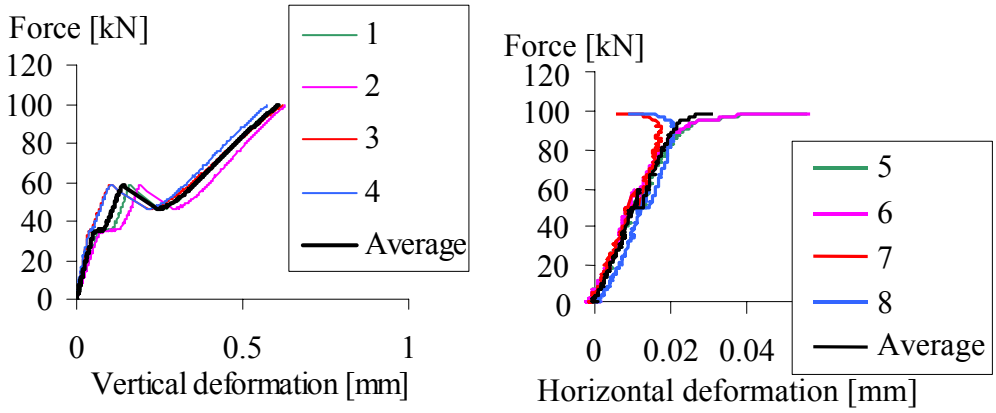

Figure B3 Measured displacements in test no. S-HR3.

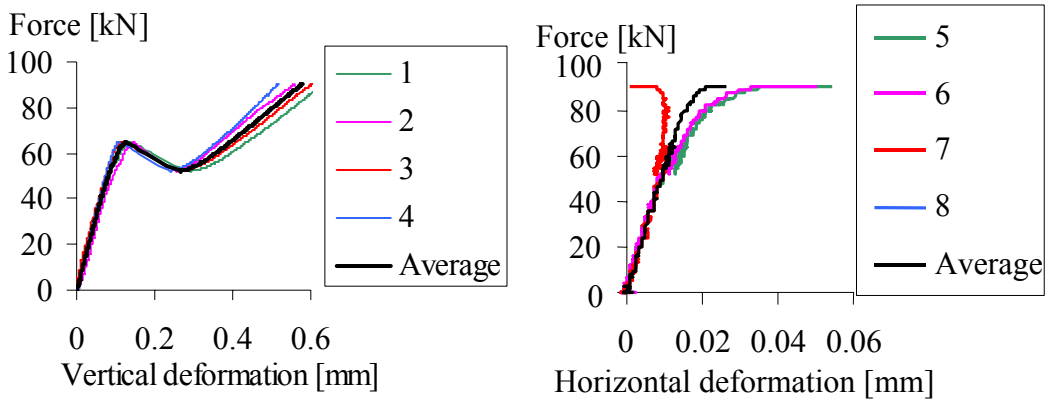

Figure B4 Measured displacements in test no. S-HR4.

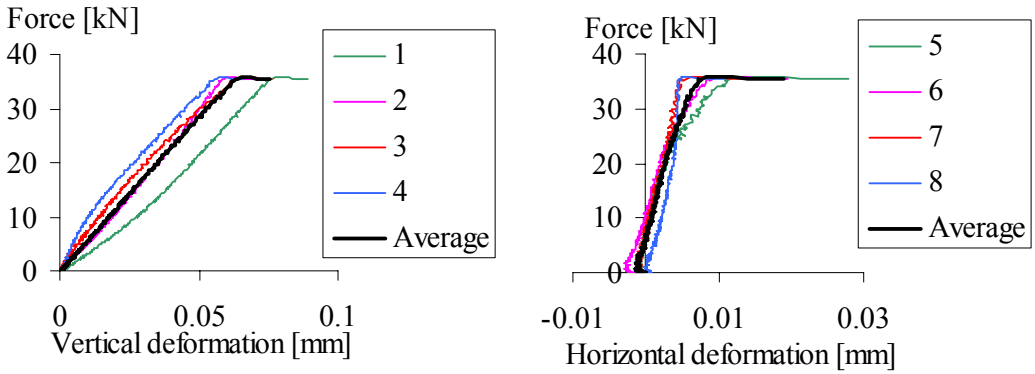

Figure B5 Measured displacements in test no. S-A1.

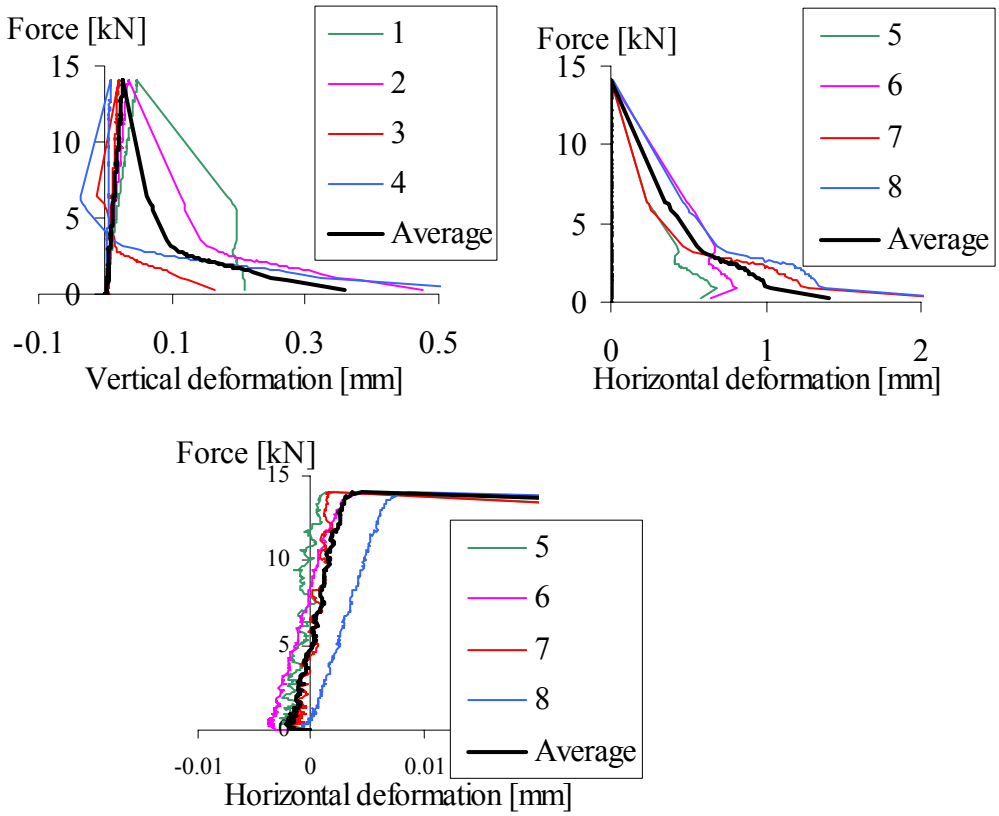

Figure B6 *Measured displacements in test no. S-A2. Horizontal deformations also shown first part enlarged.*

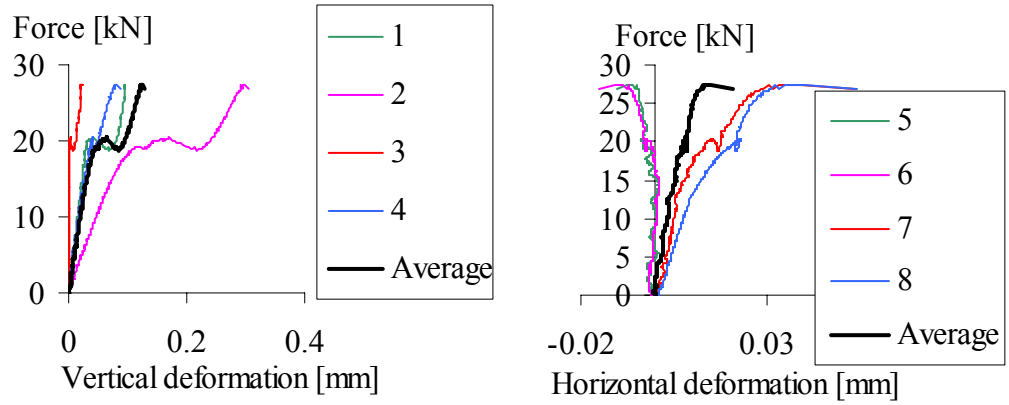

Figure B7 *Measured displacements in test no. S-A3.*

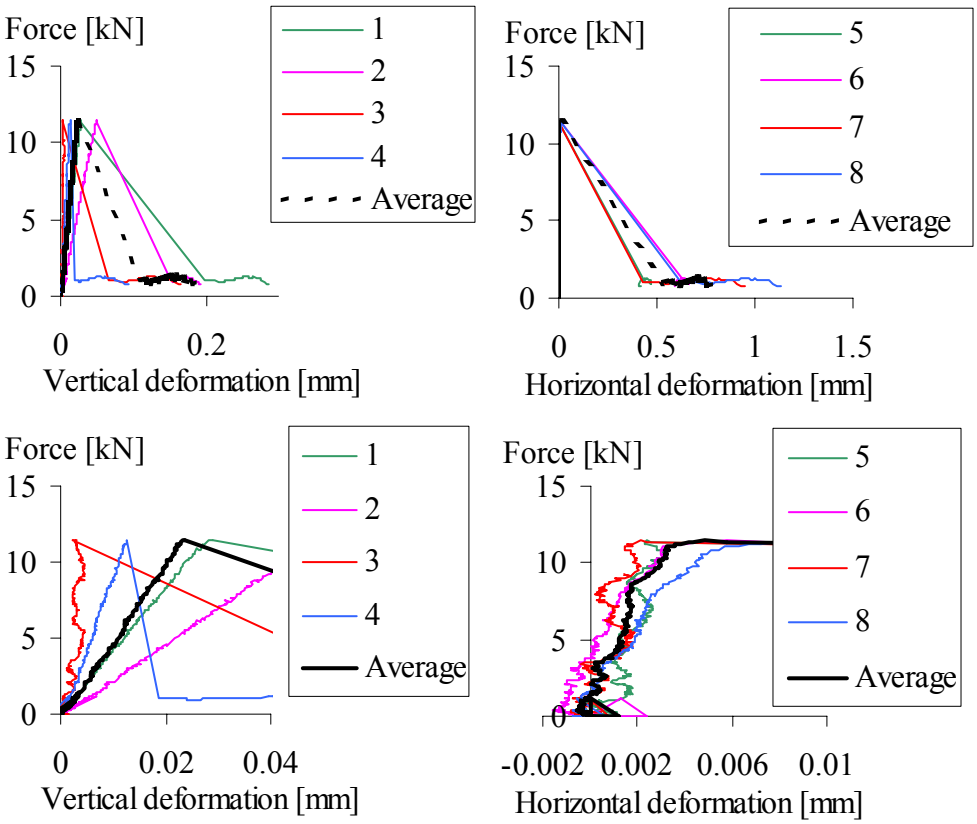

Figure B8 *Measured displacements in test no. S-A4. Both vertical and horizontal deformations also shown first part enlarged.*

Appendix C. Measured strains in full-scale tests

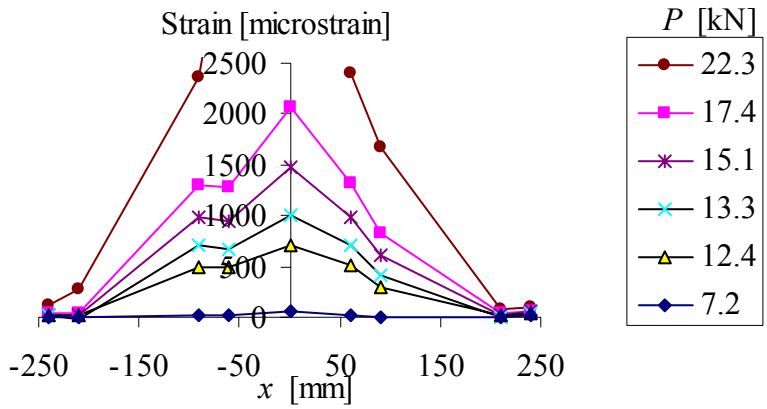

Figure C1 Measured strain in test no. A1.

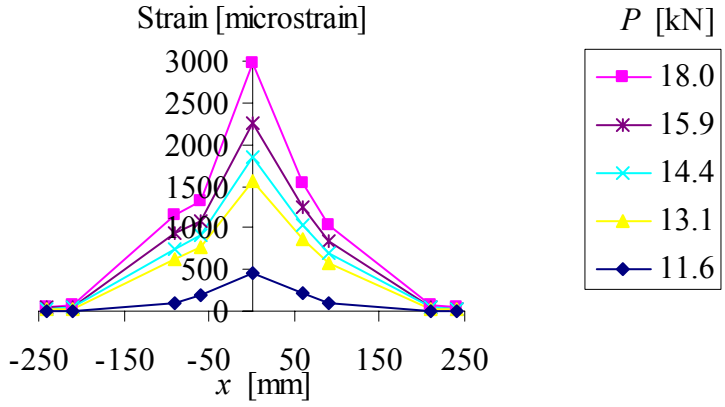

Figure C2 Measured strain in test no. A2.

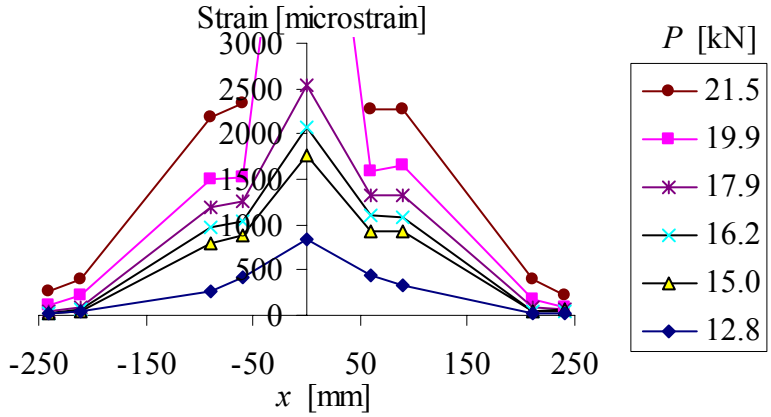

Figure C3 Measured strain in test no. A3.

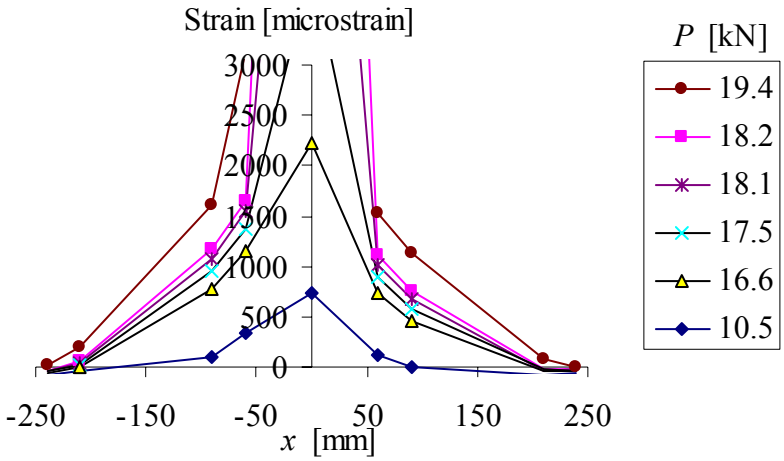

Figure C4 Measured strain in test no. H1.

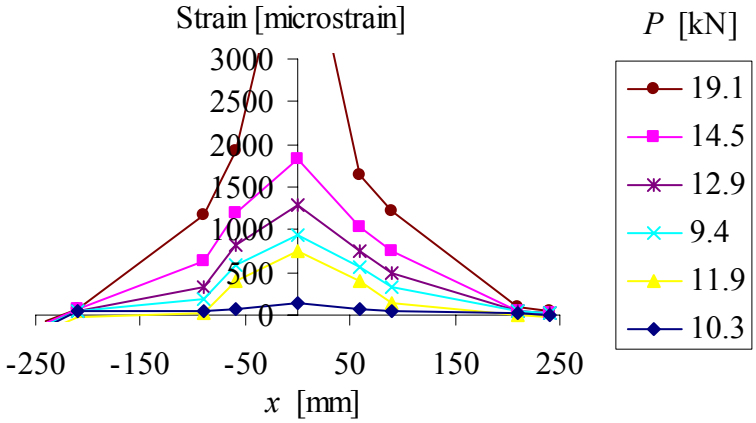

Figure C5 Measured strain in test no. H2.

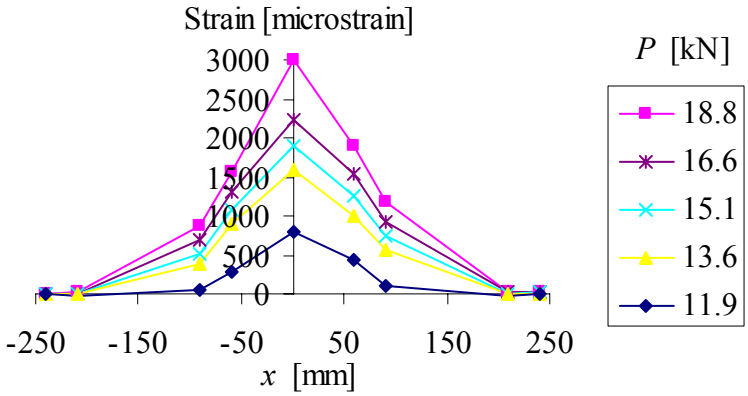

Figure C6 Measured strain in test no. H3.